

Triggered Star Formation and Evolution of T-Tauri stars in and around Bright-Rimmed Clouds

Neelam Chauhan¹, A. K. Pandey^{1*}, K. Ogura², D. K. Ojha³, B. C. Bhatt⁴,
S. K. Ghosh³, P. S. Rawat⁵

¹*Aryabhata Research Institute of Observational Sciences (ARIES), Nainital, 263 129, India*

²*Kokugakuin University, Higashi, Shibuya-ku, Tokyo 150-8440, Japan*

³*Tata Institute of Fundamental Research, Mumbai (Bombay) - 400 005, India*

⁴*CREST, Indian Institute of Astrophysics, Hosakote 562 114, India*

⁵*Physics Department, D.S.B. Campus, Kumaun University, Nainital, India*

ABSTRACT

The aim of this paper is to quantitatively testify the “*small-scale sequential star formation*” hypothesis in and around bright-rimmed clouds (BRCs). As a continuation of the recent attempt by Ogura et al. (2007, Paper I), we have carried out BVI_c photometry of four more BRC aggregates along with deeper re-observations of 2 previously observed BRCs. Again quantitative age gradients are found in almost all the BRCs studied in the present work. Archival Spitzer/IRAC data also support this result. The global distribution of NIR excess stars in each HII region studied here clearly shows evidence that a series of radiation driven implosion (RDI) processes proceeded in the past from near the central O star(s) towards the peripheries of the HII region. We found that in general weak-line T-Tauri stars (WTTs) are somewhat older than classical T-Tauri stars (CTTs). Also the fraction of CTTs among the T-Tauri stars (TTSs) associated with the BRCs is found to decrease with age. These facts are in accordance with the recent conclusion by Bertout et al. (2007) that CTTs evolve into WTTs. It seems that in general the EW of $H\alpha$ emission in TTSs associated with the BRCs decreases with age. The mass function (MF) of the aggregates associated with the BRCs of the morphological type ‘A’ seems to follow that found in young open clusters, whereas ‘B/C’ type BRCs show significantly steeper MF.

1 INTRODUCTION

It is believed that majority of the stars in the Galaxy form in clusters that may contain massive ($M \gtrsim 10M_\odot$) as well as low mass stars. A massive star has strong impact on the evolution of its parental molecular cloud. As soon as O stars form their strong ultra-violet (UV) radiation photo-ionizes the surrounding gas and develops an expanding HII region, thus dispersing the remaining molecular cloud. However, the UV radiation can also induce triggering of the next generation star formation. This phenomenon is known as ‘sequential star formation’. Observational evidence for this process is often inferred from the spatial distribution of young stars and subgroups of OB associations and their age distribution (see e.g. Sharma et al. 2007, Jose et al. 2008, Pandey et al. 2008, Samal et al. 2007).

One of the triggered star formation processes is known as the ‘collect and collapse process’, which was proposed by Elmegreen & Lada (1977). As an HII region expands the surrounding neutral material is collected between the ionization front and the shock front which precedes the former. With time the layer gets massive and consequently becomes gravitationally unstable and collapses to form stars of the second generation, including massive stars. So this process

can repeat itself. Recent simulations of this process include Hosokawa & Inutsuka (2005, 2006) and Dale et al. (2007). An observational signature of the process is the presence of a dense layer and massive condensations adjacent to an HII region (e.g., Deharveng et al. 2003).

Another process which has been frequently supported by numerical simulations as well as by observations is radiation driven implosion (RDI) of a molecular cloud condensation. In this process a pre-existing dense clump is exposed to the ionizing radiation from massive stars of the previous generation. The head part of the clump collapses due to the high pressure of the ionized gas and the self-gravity, which consequently leads to the formation of next generation stars. Detailed model calculations of the RDI process have been carried out by several authors (e.g., Bertoldi 1989, Lefloch & Lazareff 1995, Lefloch et al. 1997, De Vries et al. 2002, Kessel-Deynet & Burkert 2003, Miao et al. 2006). The signature of the RDI process is the anisotropic density distribution in a relatively small molecular cloud surrounded by a curved ionization/shock front (bright rim).

Bright-rimmed clouds (BRCs) are small molecular clouds located near the edges of evolved HII regions and show the above signature. So they are considered to be good laboratories to study the physical processes involved

in the RDI process. Actually a Submillimeter Common User Bolometer Array (SCUBA) imaging survey of the submillimeter continuum emission from BRCs has revealed the presence of embedded cores (Morgan et al. 2008, Thompson et al. 2004). Morgan et al. (2004) have shown the presence of a ionized boundary layer at the interface between the HII region and the BRC molecular cloud. They have also shown that many BRCs may be in a post-shocked state and on-going star formation, which may be due to the interaction with the external ionizing radiation. Further many BRCs are associated with the signposts of recent/ongoing star formation such as Herbig-Haro objects and Infrared Astronomical Satellite (IRAS) point sources of low temperature that meet the criteria of young stellar objects (YSOs). Sugitani, Fukui & Ogura (1991) (hereafter SFO91) and Sugitani & Ogura (1994) compiled catalogues of altogether 89 BRCs, associated with IRAS point sources for the northern and southern hemispheres, respectively. Subsequently Sugitani et al. (1995) carried out near-infrared (NIR) imaging of 44 BRCs and revealed that an elongated, small cluster or aggregate of YSOs which are aligned along the direction toward the ionizing star is often associated with them. These aggregates showed a tendency that ‘redder’ (presumably younger) stars tend to be located inside the BRCs, whereas relatively ‘bluer’ (presumably older) stars are found outside the clouds, suggesting an age gradient. Thus they advocated a hypothesis called ‘*small-scale sequential star formation*’ (S^4F), i.e. the propagation of star formation along the axis of the BRCs as the ionization/shock front advances further and further into the molecular cloud. The $H\alpha$ grism survey of 24 BRCs by Ogura et al. (2002) detected 460 $H\alpha$ emission stars (possibly, T-Tauri stars or Herbig Ae/Be stars) and 12 Herbig-Haro objects in their vicinities. Again these $H\alpha$ emission stars are found concentrated toward the head or just outside of the BRCs and aligned toward the exciting star(s) direction. Deep NIR photometry of BRC 14 by Matsuyanagi et al. (2006) revealed that three indicators of star formation, i.e., the fraction of YSOs among the sources, the amount of extinction and the near IR excesses of the YSOs, show a clear trend from outside to the inside of the rim indicating that the YSOs located near the rim are relatively younger than those located away from the rim. This result further strengthens the S^4F hypothesis.

The best way to quantitatively testify the hypothesis is to estimate the ages of the aggregate members and to compare them between different regions with respect to the bright rim. Ogura et al. (2007, hereafter referred to as Paper I) undertook BVI_c photometry of four BRC aggregates (BRCs 11NE, 12, 14 and 37) and showed that the stars inside or on the bright rim tend to have younger ages than those outside it, which is exactly what is expected from the S^4F hypothesis. The main aim of the present study is to further confirm it and to investigate the star formation scenario in/around the BRCs. We have extended BVI_c photometry to four more BRCs, namely BRCs 2, 13, 27 and 38. In addition to them we have re-observed BRCs 11NE and 14 to obtain deeper data.

The information about the observations and archival data is given in Sec. 2 and 3, respectively. Sec. 4 describes the BRCs studied in the present work. The procedure to estimate the membership, age and mass of the YSOs is described in Sec. 5. The star formation scenario, evolution of

disk of T-Tauri stars and mass functions in the BRC regions are studied in Sec. 6, 7 and 8, respectively. In sec. 9 the conclusions of the present study are summarized.

2 OBSERVATIONS AND DATA REDUCTIONS

BVI_c CCD observations of BRCs 2, 11NE, 13, 14 and 27 were carried out using the 2048×2048 pixel² CCD camera mounted on 2.0-m *Himalayan Chandra Telescope* (HCT) of the Indian Astronomical Observatory (IAO), Hanle, India on 2006 October 27 and 28. The instrument Himalaya Faint Object Spectrograph Camera (HFOSC) was used in the imaging mode. The details of the site, HCT and HFOSC can be found at the HCT website (<http://www.crest.ernet.in>). The sky at the time of observations was photometric with a seeing size (FWHM) of $\sim 1''.5$. The observations of the BRCs 2, 13, 27 were standardized on same night by observing standard stars in the SA113 field (Landolt 1992). The observations of BRCs 11NE and 14 were transformed to the standard system by using the BVI_c magnitudes given in Paper I.

The BVI_c observations of BRC 38 were obtained by using 2048×2048 pixel² CCD camera mounted at f/13 Cassegrain focus of the 1.04-m Sampurnanand Telescope (ST) at Aryabhata Research Institute of Observational Sciences (ARIES), Nainital, India. The details of the CCD camera can be found in our earlier paper (e.g. Jose et al. 2008, Pandey et al. 2008). To improve the signal to noise ratio, the observations were carried out in a binning mode of 2×2 pixels. During the observations the seeing was about $2''.1$. SA98 field of Landolt (1992) was observed on 2006, October 26 to standardize the observations. The log of the HCT and ST observations is tabulated in Table 1. A number of bias and twilight flat frames were also taken during the observing runs.

The data analysis was carried out at ARIES, Nainital, India. The initial processing of the data frames was done using various tasks available under the IRAF data reduction software package. The photometric measurements of the stars were performed using DAOPHOT II software package (Stetson 1987). The point spread function (PSF) was obtained for each frame using several uncontaminated stars. Aperture photometry was carried out for the standard stars to estimate the atmospheric extinction and to calibrate the observations. The following transformation equations were used to calibrate the observations:

$$\begin{aligned} (B - V) &= m_1(b - v) + c_1 \\ (V - I_c) &= m_2(v - i) + c_2 \\ V &= v + m_3(v - i) + c_3 \end{aligned}$$

where b , v , i are the instrumental magnitudes corrected for the atmospheric extinctions, and B , V , I_c are the standard magnitudes; c_1 , c_2 , c_3 and m_1 , m_2 , m_3 are zero-point constants and colour-coefficients, respectively. The values of the zero-point constants and the colour-coefficients are given in Table 2.

The standard deviations of the standardization residuals, Δ , between the standard and transformed magnitudes and colours of the standard stars, are found to be $\Delta V = 0.006$, $\Delta(B - V) = 0.007$ and $\Delta(V - I_c) = 0.007$ for the HCT data, whereas for the ST observations these values are 0.001, 0.010 and 0.002 respectively. The photometric accu-

Table 1. Log of optical observations

Region	Telescope	filter; exposure time(sec)×No. of frames	date of observations
BRC 2	HCT, Hanle	B : 600×4; V : 300×4; I _c : 180×4	2006.10.27
BRC 11	HCT, Hanle	B : 600×4; V : 300×4; I _c : 180×4	2006.10.28
BRC 13	HCT, Hanle	B : 600×4; V : 300×4; I _c : 180×4	2006.10.27
BRC 14	HCT, Hanle	B : 600×4; V : 300×4; I _c : 180×4	2006.10.27
BRC 27	HCT, Hanle	B : 600×4; V : 300×4; I _c : 180×4	2006.10.28
BRC 38	ST, Nainital	B : 1800×4; V : 300×8; I _c : 600×3	2006.10.26

Table 2. The zero-point constants, colour-coefficients and extinction-coefficients

Parameters	HCT	ST
Zero-point constants		
c1	-0.344 ± 0.024	-0.305 ± 0.011
c2	0.101 ± 0.005	0.541 ± 0.009
c3	-0.799 ± 0.017	-3.394 ± 0.010
colour-coefficients		
m1	0.855 ± 0.017	0.981 ± 0.008
m2	1.063 ± 0.005	0.990 ± 0.011
m3	0.078 ± 0.015	0.031 ± 0.009
Extinction-coefficients		
K _b	0.219 ± 0.009	0.301 ± 0.010
K _v	0.122 ± 0.007	0.199 ± 0.009
K _i	0.056 ± 0.008	0.088 ± 0.010

racies depend on the brightness of the stars, and the typical DAOPHOT errors in B, V and I_c bands at V ~ 18 are smaller than 0.01 mag. Near the limiting magnitude of V ~ 21, which is practically the same for HCT and ST, the DAOPHOT errors increase to 0.11, 0.05, 0.02 mag in the B, V and I_c bands, respectively. The B, V and I_c photometric data for the stars along with their positions, equivalent widths (EWs) and corresponding 2MASS data are given in Table 3.

3 ARCHIVE DATA

3.1 Near-infrared data from 2MASS

NIR *JHK_s* data for the stars in the BRC regions have been obtained from the Two Micron All Sky Survey (2MASS) Point Source Catalog (PSC) (Cutri et al. 2003). Sources having uncertainty ≤ 0.1 mag (S/N ≥ 10) in all the three bands were selected to ensure high quality data. The *JHK_s* data were transformed from the 2MASS system to the California Institute of Technology (CIT) system using the relations given in the 2MASS website. For BRC 14 we have adopted the *JHK_s* data by Matsuyanaagi et al. (2006), which were obtained with the infrared camera SIRIUS mounted on the University of Hawaii 2.2-m telescope.

3.2 Mid Infrared data from Spitzer-IRAC

We have also used archived mid-infrared (MIR) data from Infrared Array Camera (IRAC) of the *Spitzer* telescope. We obtained basic calibrated data (BCD) using the software Leopard. Mosaicking was performed using the MOPEX (Mosaicker and Point Source Extractor) software provided by

Spitzer Science Center (SSC). All of our mosaics were built at the native instrument resolution of 1".2/pixel with the standard BCDs. We used the standard IRAF photometry routines in the *apphot* package to detect sources and perform aperture photometry in each IRAC band. The FWHM of every detection is measured and all detections with FWHM > 3".6 are considered resolved and removed. The detections are also examined visually in each band to remove non-stellar objects and false detections. The sources with photometric uncertainties ≤ 0.2 mag in each band were considered as good detections. The photometry was done using an aperture radius of 3".6 and the background estimation was done within a concentric sky annulus of the inner and outer radii of 3".6 and 8".4, respectively. We adopted the zero-point magnitudes for the standard aperture radius (12") and background annulus of (12"-22".4) of 19.67, 18.93, 16.85 and 17.39 in the 3.6, 4.5, 5.8 and 8.0 μm bands, respectively. Aperture corrections were made using the values described in the IRAC Data Handbook (Reach et al. 2006).

4 DESCRIPTION OF THE BRCS STUDIED

A brief description of BRCs studied is given below.

BRC 2 : Sharpless 171 (= NGC 7822) is a large HII region associated with the Cepheus OB4 association (Yang & Fukui 1992). This region contains three BRCs, BRCs 1-3 (SFO91). A star cluster Be 59, containing nine O7-B3 stars, is located at the centre of the HII region. Recently, Pandey et al. (2008) have made photometric studies of Be 59 and its surrounding region in detail. The distance to the cluster was estimated to be 1.0 Kpc. The age of these massive stars is found to be about 1-4 Myr with an average of ~ 2 Myr. It was also found that the stars around BRC 1, which is located about 3 pc towards west of Be 59, are younger than those in the cluster. This seems to support triggered star formation in the BRC 1 region due to the massive stars in Be 59.

BRC 2 is located about 17 pc north of Be 59. On the basis of MIR observations by IRAC of the *Spitzer Space Telescope*, Megeath et al. (2004) have reported a cluster of young stars near the edge of BRC 2. The distribution of YSOs suggests that their formation is triggered by a photo-evaporation driven shock propagating into the BRC 2 cloud.

BRCs 11NE, 13 and 14 : The large H II region IC 1848 = S199, associated with the radio source W5, is located in the Perseus arm at the distance of about 1.9 kpc (SFO91). In fact it is composed of two adjacent HII regions namely, IC 1848W and IC 1848E Vallee et al. 1979, Karr & Martin 2003, Koenig et al. 2008). IC 1848W is ionized by HD 17505 (O6V) and HD 17520 (O9V), whereas IC 1848E is

ionized by HD 18326 (O7V). The former harbours a young cluster (age ~ 1 Myr; Feinstein et al. 1986). Carpenter et al. (2000) reported several deeply embedded star forming sites in the W3/W4/W5 region and put forward the notion of triggered star formation in this complex. Based on a multi-wavelength study of the W5 star forming region, Karr & Martin (2003) investigated the star formation scenario and supported triggered star formation in this region.

SFO91 lists four BRCs, BRCs 11 - 14 around IC 1848. BRC 11 is situated near the southern edge of IC 1848W, BRC 12 near its northern edge and BRCs 13 and 14 at the eastern edge of IC 1848E. There are two more BRCs in the vicinity of BRC11, which are designated as BRC 11NE and BRC 11E, respectively, by Ogura et al. (2002). They are not listed in SFO91 because of the lack of associated IRAS point sources. However, Ogura et al. (2002) found several H α emission stars in the vicinity of BRC 11NE in contrast to one or two in and around BRC 11 and BRC 11E. Moreover BRC 11NE appears to be associated with a more or less clear aggregate of young stars just outside its tip. So BRC 11NE was selected as one of the target BRCs in Paper I to show an age gradient. In the present study we have aimed to increase the sample stars for age determination by reaching a deeper limiting magnitude.

BRC 14 is associated with the molecular cloud IC 1848A to its east, which harbours a bright infrared young cluster AFGL 4029 (Deharveng et al. 1997). The optical and NIR study by these authors revealed that AFGL 4029 is an active star formation site. A deeper NIR survey of the BRC 14 region by Matsuyanagi et al. (2006) supports sequential star formation in this region propagating from the west. Paper I determined the ages of the stars associated with BRC 14 and found a quantitative evidence for the S^4F hypothesis. We are repeating the study with deeper data for this BRC too.

BRC 27 : BRC 27 is located at the outer edge of S296 at a distance of 1.15 Kpc (SFO91) and associated with the active star forming region Canis Major R1 (CMa R1). The location of S296 coincides with the boundary of an expanding neutral hydrogen shell. Shevchenko et al. (1999) have estimated the ages of the stellar contents of CMa R1 ranging from < 1 Myr to 8 Myr. Herbst & Assoua (1977) suggested that the star formation in the CMa R1 region could have been triggered by a supernova explosion.

BRC 38 : Cepheus OB2, located at a distance of ~ 870 pc (Contreras et al. 2002), is a complex of a stellar aggregate and a bubble-shaped structure of atomic and molecular gas (Patel et al. 1994, 1998). The clusters NGC 7160 and Tr 37 are located near the centre of the bubble and near its edge, respectively. There is evidence that the star formation at the edge of the bubble was triggered by a supernova explosion which took place near the centre of the bubble (Sicilia-Aguilar et al. 2004, 2005). Tr 37 harbours an O6 star HD 206267, which excites the relatively evolved HII region IC 1396. The age of Tr 37 is estimated as ~ 3 -5 Myr (Contreras et al. 2002). IC 1396 has a rich population of BRCs including BRCs 32-42 (SFO91), among which BRCs 37 and 38 have been studied extensively (see, e.g., Getman et al 2007 and Ikeda et al. 2008). In particular, Paper I reported quantitative evidence for S^4F in BRC 37, and Ikeda et al. (2008) confirmed sequential star formation in this region.

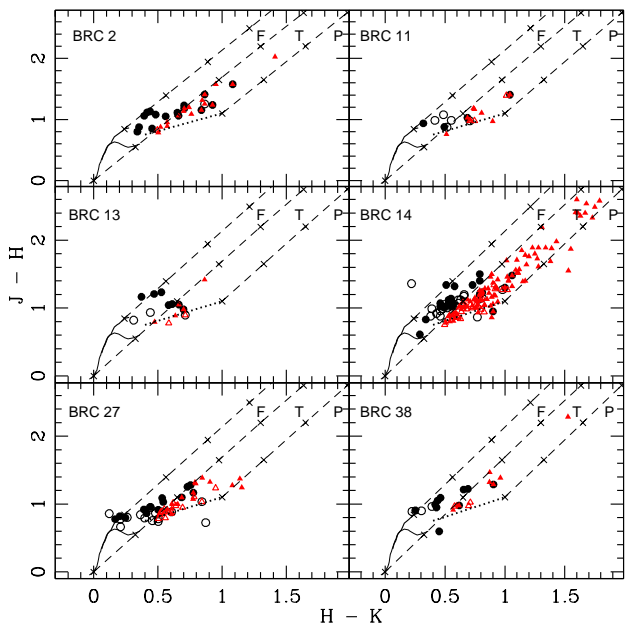


Figure 1. $(J-H)/(H-K)$ colour-colour diagrams for BRCs 2, 11NE, 13, 14, 27 and 38. The sequences for dwarfs (thin solid curve) and giants (thick solid curve) are from Bessel & Brett (1988). The dotted line represents the intrinsic locus of CTTs (Meyer et al. 1997). The three parallel dashed lines represent the reddening vectors. The crosses on the dashed lines are separated by $A_V = 5$ mag. The open and filled circles are H α emission stars lying in outside and on/inside the bright rims (see Fig. A1) respectively. The open and filled triangles are NIR excess stars lying in outside and on/inside the bright rims respectively.

Getman (2007) provided detailed qualitative discussion on S^4F based on the *Chandra* X-ray data for BRC 38.

5 MEMBERSHIP AND AGE DETERMINATION OF MEMBER STARS

The aggregates associated with BRCs are very loose and are composed of a small number of stars. Since BRCs are found at low galactic latitudes, the fields can be significantly contaminated by foreground/background stars. To understand star formation in BRCs it is necessary to identify stars directly related to them. We selected probable members associated with the BRCs using the following criteria.

The spectra of some pre-main sequence (PMS) stars, specifically CTTs, show emission lines, among which usually H α is the strongest. Therefore, H α emission stars can be considered as good candidates for PMS stars associated with BRCs. In the present study we use H α emission stars found by Ogura et al. (2002) in the vicinity of BRCs. However, some of them may not be directly associated with the BRCs (see Sec 6.3).

Since many PMS stars also show NIR excesses caused by circumstellar disks, NIR photometric surveys have also emerged as a powerful tool to detect low-mass PMS stars. To identify NIR excess stars from the 2MASS PSC, we used NIR $(J-H)/(H-K)$ colour-colour (NIR-CC) diagrams. Figure 1 shows NIR-CC diagrams for the studied BRCs. The thin and thick solid curves represent the unreddened main-

sequence and giant branches (Bessell & Brett 1988), respectively. The dotted line indicates the locus of intrinsic CTTSs (Meyer et al. 1997). The curves are also in the CIT system. The parallel dashed lines are the reddening vectors drawn from the tip (spectral type M4) of the giant branch (“upper reddening line”), from the base (spectral type A0) of the main-sequence branch (“middle reddening line”) and from the tip of the intrinsic CTTS line (“lower reddening line”). The extinction ratios $A_J/A_V = 0.265$, $A_H/A_V = 0.155$ and $A_K/A_V = 0.090$ have been adopted from Cohen et al. (1981). We classified sources into three regions in the NIR-CC diagrams (cf. Ojha et al. 2004a). ‘F’ sources are located between the upper and middle reddening lines and are considered to be either field stars (main-sequence stars, giants) or Class III and Class II sources with small NIR excesses. ‘T’ sources are located between the middle and lower reddening lines. These sources are considered to be mostly CTTSs (Class II objects). There may be an overlap in NIR colours of Herbig Ae/Be stars and CTTSs in the ‘T’ region (Hillenbrand et al. 1992). ‘P’ sources are those located in the region redward of the ‘T’ region and are most likely Class I objects (protostar-like objects; Ojha et al. 2004b). So, objects falling in the ‘T’ and ‘P’ regions of NIR-CC diagrams are considered as NIR excess stars and probable members of the BRC aggregates. These are included in the analysis of the present study in addition to H α emission stars. However, we selected only those H α emission stars, as probable members associated with the BRCs, that lie rightward of the upper reddening line. It is worthwhile, however, to mention that Robitaille et al. (2006) have recently shown that there is a significant overlap between protostars and CTTSs in the NIR-CC space.

The spatial distribution of the probable YSOs (i.e., H α emission and NIR excess stars) for each BRC is shown in Fig. A1, which is available in electronic form only. In Fig. A1 we have also demarcated the two regions for each BRC, i.e., on/inside and outside the bright rim. The NIR-CC diagrams (Fig. 1) were used to estimate A_V for each of these stars by tracing back to the intrinsic CTTS line of Meyer et al. (1997) along the reddening vector (for details see, Paper I). The A_V for stars lying in the ‘F’ region is estimated by tracing them back to the extension of the intrinsic CTTS line. Fig. 2 shows dereddened V_0 , $(V - I_c)_0$ colour-magnitude (CM) diagrams for those stars.

In Fig. 2 the post-main sequence isochrone for 2 Myr by Girardi et al. (2002), which is practically a ZAMS line, and PMS isochrones for 1, 3, 10, 30 Myr for the solar metallicity by Siess et al. (2000) are also plotted. The distances are taken from SFO 91 barring for BRC 38. In the case of BRC 38 a distance of 870 pc has been adopted from Contreras et al. (2002). The age of each YSO was estimated by referring to the isochrones. The mass of the YSOs was estimated using the $V_0/(V - I_c)_0$ colour-magnitude diagram as discussed in Pandey et al. (2008). The resultant A_V values, ages and masses are given in Table 4.

The ages range from 0.1 to a few Myr (with some exceptions) which are comparable with the lifetime of T-Tauri stars (TTs). The masses of these YSOs, range from ~ 0.1 - $2.0 M_\odot$, further indicate that they are probable TTs and their siblings.

Here we would like to point out that the estimation of the ages of the PMS stars by comparing the observa-

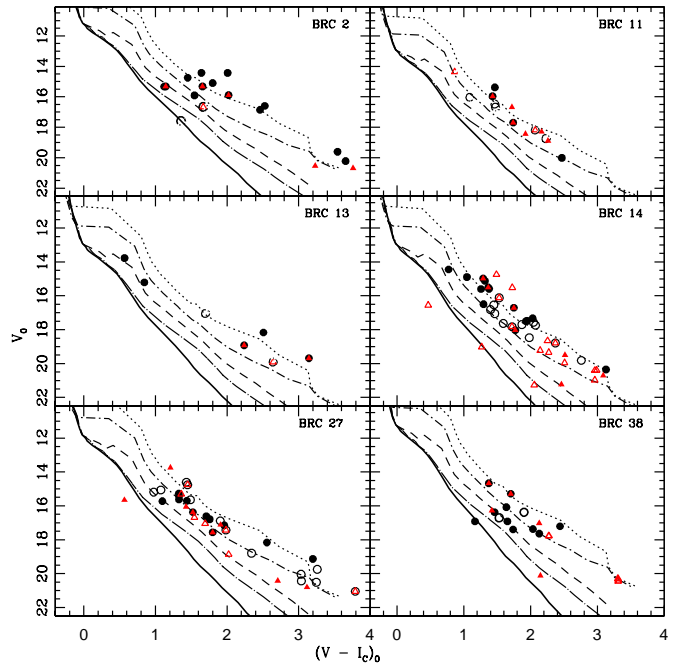


Figure 2. $V_0/(V - I_c)_0$ colour-magnitude diagrams for probable YSOs in BRCs 2, 11NE, 13, 14, 27 and 38. The 2 Myr isochrone (thick curve) by Girardi et al. (2002) and PMS isochrones of 1 (dotted), 3 (dashed-dotted), 10 (dashed), 30 (large dashed-dotted) Myr by Siess et al. (2000) are also shown. All the isochrones are corrected for the distances of the respective BRCs. The symbols are same as in Fig. 1.

tions with the theoretical isochrones is prone to two kinds of errors; random errors in observations and systematic errors due to the variation between the predictions of different theoretical evolutionary tracks (see e.g. Hillenbrand 2005). The effect of random errors in determination of A_V , age and mass was estimated by propagating the random errors to the observed estimation by assuming normal error distribution and using the Monte-Carlo simulations. The use of different PMS evolutionary model gives different age and age spread in a cluster (e.g. Sung et al. 2000). Here in the present study we have used model by Siess et al. (2000) only for all the BRCs, therefore our age and mass estimations are not affected by the systematic errors. However, the use of different sets of PMS evolutionary tracks will introduce systematic shift in age determination. The presence of binaries may be the another source of error in the age determination. The presence of binary will brighten a star, consequently the CMD will yield a lower age estimate. In the case of equal mass binary we expect an error of ~ 50 - 60% in age estimation of the PMS stars. However, it is difficult to estimate the influence of binaries on mean age estimation as the fraction of binaries is not known. Here we would like to point out that we are interested mainly in the *relative* ages of the aggregate members, in particular, the spatial differences with respect to the bright rim.

6 STAR FORMATION SCENARIO IN BRC REGIONS

Propagating star formation, where energetic activity of massive stars compresses the surrounding gas and triggers the

Table 4. Dereddened magnitude, colours, age, and mass of the YSOs associated with the BRCs.

S.No.	RA (2000)	DEC (2000)	V ₀ (mag)	(B-V) ₀ (mag)	(V-I) ₀ (mag)	A _V ± σ (mag)	Age ± σ (Myr)	Mass ± σ (M _⊙)	ID(Ogura et al. 2002)
BRC 2									
1	00 03 57.1	+68 33 46.4	15.101	1.149	1.800	3.0 ± 0.4	0.7 ± 0.0	0.52 ± 0.01	5
2	00 03 57.3	+68 33 23.0	19.604	-	3.543	2.9 ± 0.5	0.3 ± 0.0	0.14 ± 0.01	6
3	00 03 59.1	+68 32 47.4	20.219	-	3.656	0.9 ± 0.5	0.3 ± 0.0	0.11 ± 0.01	8
4	00 04 01.6	+68 34 14.2	15.911	-	1.546	2.1 ± 0.5	4.0 ± 0.9	0.78 ± 0.06	9
5	00 04 01.8	+68 34 00.1	16.857	-	2.460	5.9 ± 0.5	1.1 ± 0.1	0.30 ± 0.02	10
6	00 04 01.8	+68 34 34.3	14.431	1.246	2.008	2.5 ± 0.6	0.1 ± 0.0	0.47 ± 0.01	12
7	00 04 02.6	+68 34 26.0	15.329	-	1.123	4.2 ± 0.6	16.1 ± 3.0	1.11 ± 0.04	14
8	00 04 07.6	+68 33 24.8	14.750	0.995	1.451	4.9 ± 0.4	1.2 ± 0.1	0.85 ± 0.03	21
9	00 04 11.7	+68 33 25.2	16.596	-	2.527	3.9 ± 0.4	0.2 ± 0.1	0.29 ± 0.00	22
10	00 04 15.2	+68 33 01.8	14.428	1.170	1.643	2.2 ± 0.4	0.6 ± 0.0	0.63 ± 0.01	25
11	00 03 58.4	+68 34 06.6	15.320	-	1.144	5.4 ± 0.4	12.3		7
12	00 04 04.6	+68 34 52.0	15.891	1.298	2.022	3.5 ± 0.4	0.9 ± 0.0	0.40 ± 0.01	16
13	00 04 05.6	+68 33 44.3	15.319	-	1.658	2.0 ± 0.4	1.2 ± 0.1	0.63 ± 0.02	19
14	00 03 38.0	+68 34 55.6	20.526	-	3.231	0.7 ± 0.6	4.5 ± 0.2	0.14 ± 0.02	
15	00 03 54.5	+68 33 43.2	20.680	-	3.761	2.2 ± 0.4	1.0	0.09 ± 0.01	
16	00 04 14.0	+68 32 21.5	16.680	0.921	1.665	3.2 ± 0.5	6.7 ± 1.1	0.68 ± 0.03	23
17	00 04 14.7	+68 32 48.8	17.600	-	1.355	4.3 ± 0.4	>30		24
BRC 11NE									
18	02 51 37.4	+60 06 26.6	16.495	1.028	1.463	2.0 ± 0.6	1.5 ± 0.2	0.91 ± 0.01	1
19	02 51 54.5	+60 08 26.6	18.196	1.485	2.065	0.6 ± 0.6	1.3 ± 0.1	0.44 ± 0.01	4
20	02 51 58.7	+60 08 05.8	18.760	1.421	2.226	0.7 ± 0.5	1.5 ± 0.1	0.35 ± 0.01	5
21	02 52 11.1	+60 07 15.2	16.047	0.674	1.087	3.8 ± 0.7	4.5 ± 0.8	1.45 ± 0.05	7
22	02 52 15.1	+60 05 18.5	16.692	0.557	1.471	3.1 ± 0.6	1.5 ± 0.2	0.83 ± 0.04	8
23	02 51 54.2	+60 07 43.5	15.384	0.927	1.465	3.2 ± 0.5	0.5 ± 0.0	0.96 ± 0.03	3
24	02 51 59.7	+60 06 39.3	17.693	1.172	1.739	1.5 ± 0.6	1.7 ± 0.2	0.58 ± 0.02	6
25	02 51 52.1	+60 07 10.0	16.677	1.157	1.720	1.7 ± 0.4	0.7 ± 0.1	0.59 ± 0.03	
26	02 52 01.3	+60 06 15.3	18.891	-	2.261	3.0 ± 0.7	1.7 ± 0.1	0.34 ± 0.01	
27	02 51 59.9	+60 05 32.0	18.437	-	1.924	3.3 ± 1.1	2.1 ± 0.5	0.46 ± 0.03	
BRC 11									
28	02 51 32.8	+60 03 54.3	15.967	-	1.431	3.9 ± 0.4	0.9 ± 0.1	0.97 ± 0.03	1
29	02 51 25.6	+60 06 04.8	14.372	0.353	0.860	4.0 ± 0.5	2.7 ± 0.3	2.2 ± 0.08	
BRC 11E									
30	02 52 13.6	+60 03 26.2	20.008	-	2.468	1.0 ± 0.9	2.9 ± 0.3	0.27 ± 0.01	1
31	02 52 14.2	+60 03 11.7	18.291	0.347	2.165	0.8 ± 0.5	1.2 ± 0.1	0.36 ± 0.01	
BRC 13									
32	03 00 51.1	+60 39 36.3	15.917	0.887	-	2.6 ± 0.6	8.0 ± 1.3	1.45 ± 0.04	6
33	03 00 51.6	+60 39 48.9	19.684	-	3.144	2.00 ± 0.6	0.1 ± 0.0	0.19 ± 0.01	7
34	03 00 52.7	+60 39 31.6	18.923	1.371	2.239	0.7 ± 0.6	1.7 ± 0.1	0.34 ± 0.01	10
35	03 00 53.6	+60 40 24.9	13.770	0.492	0.569	5.9 ± 0.6	8.6 ± 0.8	1.72 ± 0.04	11
36	03 00 55.4	+60 39 42.7	15.210	-	0.845	5.6 ± 0.9	8.0 ± 1.4	1.41 ± 0.05	12
37	03 00 56.0	+60 40 26.3	18.169	-	2.508	2.5 ± 0.7	0.1 ± 0.0	0.29 ± 0	13
38	03 00 44.8	+60 40 09.1	19.923	1.974	2.640	0 ± 0.5	2.2 ± 0.1	0.36 ± 0.00	2
39	03 00 45.3	+60 40 39.5	17.059	1.329	1.695	1.7 ± 0.5	1.0 ± 0.1	0.60 ± 0.02	3
BRC 14									
40	03 01 24.0	+60 30 42.2	17.480	-	1.947	3.9 ± 0.1	0.9 ± 0.0	0.45 ± 0.02	29
41	03 01 24.7	+60 30 09.6	15.586	-	1.379	6.4 ± 0.1	0.7 ± 0.1	0.98 ± 0.08	30
42	03 01 25.6	+60 29 39.0	15.597	-	1.258	4.1 ± 0.1	1.1 ± 0.1	1.20 ± 0.01	31
43	03 01 26.4	+60 30 53.9	15.126	1.068	1.317	3.2 ± 0.1	0.5 ± 0.0	1.10 ± 0.0	32
44	03 01 27.2	+60 30 56.9	18.031	-	1.771	2.9 ± 0.3	2.3 ± 0.2	0.56 ± 0.02	33
45	03 01 27.4	+60 30 39.7	16.498	0.899	1.295	4.2 ± 0.1	2.7 ± 0.3	1.11 ± 0.04	34
46	03 01 29.3	+60 31 13.6	15.511	1.001	1.366	2.8 ± 0.1	0.7 ± 0.1	0.99 ± 0.01	35
47	03 01 34.0	+60 27 45.6	17.503	1.428	1.931	2.9 ± 0.1	0.9 ± 0	0.45 ± 0.01	39
48	03 01 34.4	+60 30 08.5	14.977	-	1.290	5.5 ± 0.1	0.5 ± 0.0	1.19 ± 0.03	40
49	03 01 36.4	+60 29 06.1	16.706	-	1.749	4.8 ± 0.1	0.7 ± 0.0	0.55 ± 0.03	41
50	03 01 37.0	+60 31 00.2	17.326	-	2.031	3.1 ± 0.1	0.7 ± 0.0	0.39 ± 0.01	42
51	03 01 37.1	+60 29 41.2	20.355	-	3.128	0 ± 0.2	0.3 ± 0.0	1.80 ± 0.00	43
52	03 01 43.3	+60 28 51.5	14.893	-	1.047	7.2 ± 0.1	1.4 ± 0.3	1.79 ± 0.11	46

Table 4 cont.

53	03 01 50.0	+60 28 50.5	14.444	-	0.773	7.3 ± 0.1	5.6 ± 1.7	1.90 ± 0.18	47
54	03 01 04.2	+60 31 25.3	16.820	-	1.400	3.8 ± 0.1	2.4 ± 0.2	0.94 ± 0.03	1
55	03 01 06.2	+60 30 17.6	17.572	0.763	2.043	3.1 ± 0.1	0.9 ± 0.1	0.29 ± 0.01	3
56	03 01 06.6	+60 30 36.0	19.819	-	2.760	2.5 ± 0.3	1.5 ± 0.3	0.26 ± 0.01	4
57	03 01 07.7	+60 29 21.8	16.119	1.233	1.530	2.2 ± 0.1	0.8 ± 0.0	0.75 ± 0.00	5
58	03 01 11.5	+60 30 46.3	18.474	-	1.981	2.4 ± 0.3	1.8 ± 0.2	0.42 ± 0.04	6
59	03 01 13.4	+60 29 31.9	17.696	-	1.871	4.1 ± 0.1	1.2 ± 0.1	0.48 ± 0.02	8
60	03 01 16.1	+60 29 47.1	17.738	-	2.075	3.4 ± 0.1	0.9 ± 0.0	0.38 ± 0.01	10
61	03 01 17.0	+60 29 23.2	16.532	1.359	1.451	3.4 ± 0.1	1.3 ± 0.1	0.85 ± 0.02	12
62	03 01 20.3	+60 30 02.3	17.826	-	1.723	2.5 ± 0.1	2.1 ± 0.1	0.59 ± 0.01	18
63	03 01 20.6	+60 29 31.7	17.630	0.904	1.592	3.1 ± 0.1	3.1 ± 0.3	0.72 ± 0.02	20
64	03 01 21.2	+60 29 44.3	17.052	-	1.464	3.3 ± 0.1	2.4 ± 0.2	0.85 ± 0.03	23
65	03 01 21.2	+60 30 10.5	18.789	-	2.372	2.2 ± 0.1	1.3 ± 0.0	0.33 ± 0.01	24
66	03 01 32.0	+60 29 36.3	21.235	-	2.460	0.7 ± 0.3	9.0 ± 1.2	0.23 ± 0	
67	03 01 21.9	+60 29 29.5	19.493	-	2.515	1.1 ± 0.9	1.7 ± 0.2	0.28 ± 0.01	
68	03 01 51.4	+60 27 22.7	20.701	-	3.087	1.6 ± 0.9	0.9 ± 0.7	0.17 ± 0.01	
69	03 01 19.4	+60 29 38.9	21.266	-	2.055	0.7 ± 0.2	>30		
70	03 00 47.1	+60 28 53.6	19.343	-	2.273	1.0 ± 0.7	2.3 ± 0.2	0.33 ± 0.01	
71	03 01 20.3	+60 29 49.3	14.746	1.183	1.490	0 ± 0.4	0.3 ± 0.1	0.89 ± 0.04	
72	03 01 23.5	+60 31 50.6	19.226	-	2.143	1.6 ± 1.2	2.6 ± 0.5	0.36 ± 0.02	
73	03 01 14.1	+60 29 37.4	21.553	-	2.357	0 ± 0.1	>15		
74	03 01 01.1	+60 30 45.2	19.026	-	1.269	2.0 ± 0.1	>30		
75	03 00 58.0	+60 30 13.4	18.655	-	2.253	1.1 ± 0.6	1.4 ± 0.1	0.35 ± 0.01	
76	03 01 00.9	+60 33 26.7	20.402	-	2.989	0.3 ± 1.1	1.8 ± 0.4	0.21 ± 0.01	
77	03 01 02.9	+60 31 22.4	20.978	-	2.961	0.1 ± 1.3	2.8 ± 0.3	0.17 ± 0.02	
78	03 00 57.9	+60 31 21.7	20.406	-	2.961	0.4 ± 0.0	1.8	0.19	
79	03 00 51.8	+60 32 10.8	19.960	-	2.510	0.8 ± 1.3	2.6 ± 0.4	0.27 ± 0.01	
80	03 01 05.2	+60 31 55.4	15.523	1.334	1.727	0.8 ± 0.3	0.1 ± 0.0	0.61 ± 0.01	
BRC 27									
81	07 03 52.8	-11 23 13.2	15.278	0.860	1.326	2.2 ± 0.6	2.0 ± 0.5	1.05 ± 0.09	2
82	07 03 53.8	-11 24 28.4	18.164	-	2.557	1.9 ± 0.6	1.4 ± 0.1	0.29 ± 0.01	4
83	07 03 57.1	-11 24 32.8	16.618	0.920	1.711	2.5 ± 0.4	1.9 ± 0.2	0.60 ± 0.01	7
84	07 04 02.9	-11 23 37.3	15.426	0.642	1.330	3.6 ± 0.6	2.3 ± 0.5	1.03 ± 0.08	8
85	07 04 03.1	-11 23 50.6	15.726	-	1.097	4.5 ± 0.7	11.2 ± 1.1	1.19 ± 0.01	10
86	07 04 04.3	-11 23 55.7	17.151	0.637	1.962	2.5 ± 0.6	1.5 ± 0.2	0.44 ± 0.01	12
87	07 04 04.8	-11 23 39.8	15.620	0.920	1.329	2.7 ± 0.5	3.0 ± 0.5	1.06 ± 0.55	14
88	07 04 05.3	-11 23 13.2	16.378	0.660	1.523	2.7 ± 0.9	3.4 ± 0.8	0.80 ± 0.05	15
89	07 04 06.0	-11 23 58.9	16.791	1.188	1.758	1.4 ± 0.4	1.9 ± 0.2	0.56 ± 0.02	16
90	07 04 06.0	-11 23 15.7	17.568	-	1.800	2.5 ± 0.7	4.5 ± 0.8	0.54 ± 0.03	17
91	07 04 06.5	-11 23 36.2	19.134	-	3.199	1.5 ± 0.6	0.2 ± 0.0	0.18 ± 0.01	18
92	07 04 06.5	-11 23 16.4	15.700	0.933	1.439	2.4 ± 0.7	1.9 ± 0.3	0.88 ± 0.04	19
93	07 03 52.6	-11 26 16.8	15.064	0.907	1.076	1.8 ± 0.4	5.3 ± 0.4	1.43 ± 0.02	1
94	07 03 55.0	-11 25 14.5	16.887	1.067	1.906	1.9 ± 0.5	1.4 ± 0.1	0.47 ± 0.01	5
95	07 03 56.4	-11 25 41.5	20.435	-	3.039	0 ± 0.9	3.2 ± 1.4	0.14 ± 0.01	6
96	07 04 04.1	-11 26 35.5	20.515	-	3.247	0 ± 0.8	0.9	0.11 ± 0.01	11
97	07 04 08.2	-11 23 54.6	15.644	1.136	1.488	0.3 ± 0.5	1.5 ± 0.1	0.81 ± 0.02	22
98	07 04 08.2	-11 23 09.6	18.795	1.066	2.343	1.5 ± 1.1	3.2 ± 0.5	0.30 ± 0.01	23
99	07 04 09.4	-11 24 38.1	21.053	-	3.792	0 ± 0.6	0.3 ± 0.1	0.10 ± 0.00	24
100	07 04 09.8	-11 23 16.4	14.759	1.039	1.449	0.4 ± 0.3	0.6 ± 0.1	0.85 ± 0.02	25
101	07 04 12.0	-11 24 23.0	19.751	-	3.261	0.6 ± 0.7	0.3 ± 0.0	0.14 ± 0.00	27
102	07 04 13.0	-11 24 03.2	15.189	0.744	0.976	2.4 ± 0.7	9.4 ± 2.5	1.34 ± 0.07	28
103	07 04 13.4	-11 24 55.8	14.604	1.043	1.432	0.9 ± 0.3	0.6 ± 0.1	0.89 ± 0.02	29
104	07 04 14.2	-11 23 17.2	17.430	1.365	1.985	0.2 ± 0.3	1.9 ± 0.1	0.42 ± 0.01	31
105	07 04 14.2	-11 23 37.3	20.043	-	3.034	0.8 ± 0.8	2.9 ± 0.3	0.18 ± 0.01	32
106	07 04 08.4	-11 20 05.3	17.122	1.258	1.909	1.7 ± 0.4	1.7 ± 0.1	0.46 ± 0.01	
107	07 04 03.1	-11 23 27.6	13.749	-	1.209	5.2 ± 0.5	0.6 ± 0.1	1.38 ± 0.06	
108	07 03 54.7	-11 20 11.0	20.425	-	2.709	1.0 ± 1.0	6.3 ± 0.9	0.2 ± 0.01	
109	07 03 52.3	-11 21 01.1	20.808	-	3.117	1.4 ± 0.9	4.0 ± 0.4	0.11 ± 0.01	
110	07 04 12.2	-11 20 20.8	15.657	-	0.567	4.7 ±	>30		
111	07 04 05.8	-11 20 03.8	16.059	-	1.428	4.4 ± 0.6	3.5 ± 1.2	0.92 ± 0.09	
112	07 04 16.8	-11 24 32.4	16.685	0.669	1.545	0.3 ± 0.4	4.7 ± 0.5	0.79 ± 0.02	
113	07 04 15.1	-11 26 22.6	15.313	0.868	1.362	1.9 ± 0.4	1.7 ± 0.2	0.97 ± 0.05	
114	07 04 19.9	-11 22 22.4	17.050	0.979	1.695	1.2 ± 0.3	3.7 ± 0.4	0.63 ± 0.02	
115	07 04 15.1	-11 23 39.8	18.869	-	2.023	1.8 ± 1.0	8.9 ± 2.4	2.02 ± 0.02	

Table 4 cont.

BRC 38									
116	21 40 26.2	+58 14 24.7	16.917	1.035	1.168	3.3 ±0.8	>30		1
117	21 40 28.1	+58 15 14.4	16.375	-	1.460	3.8 ±0.5	11.3 ±1.9	0.87 ±0.03	3
118	21 40 31.7	+58 17 55.3	16.082	1.119	1.637	4.2 ±0.4	3.1 ±0.4	0.67 ±0.02	4
119	21 40 37.0	+58 14 38.0	15.288	1.382	1.704	1.4 ±0.4	0.9 ±0.0	0.59 ±0.02	6
120	21 40 37.0	+58 15 03.2	17.644	1.086	2.130	2.5 ±0.5	3.0 ±0.3	0.36 ±0.01	7
121	21 40 41.3	+58 15 11.5	14.673	0.917	1.374	3.4 ±0.4	1.5 ±0.2	0.95 ±0.04	9
122	21 40 41.5	+58 14 25.8	17.398	0.913	1.738	3.2 ±0.4	12.3 ±1.8	0.61 ±0.02	10
123	21 40 44.9	+58 15 03.6	16.921	-	1.653	4.3 ±0.5	9.5 ±2.1	0.7 ±0.04	11
124	21 40 48.0	+58 15 37.8	17.209	1.005	2.441	3.3 ±0.4	1.3 ±0.1	0.3	12
125	21 40 49.0	+58 17 09.6	17.374	-	2.035	4.2 ±0.5	2.9 ±0.4	0.39 ±0.02	15
126	21 40 27.4	+58 14 21.5	16.709	0.625	1.530	3.0 ±0.5	11.9 ±2.5	0.8 ±0.02	2
127	21 40 36.5	+58 13 46.2	16.379	1.331	1.902	2.8 ±0.4	1.5 ±0.1	0.47 ±0.01	5
128	21 40 42.7	+58 19 37.6	17.030	-	2.129	4.1 ±0.4	1.7 ±0.1	0.37 ±0.01	
129	21 41 12.0	+58 20 33.7	20.125	-	2.148	1.6 ±1.2	>30		
130	21 40 45.1	+58 19 50.2	16.277	-	1.421	6.1 ±0.4	10.2	0.84 ±0.03	
131	21 39 49.2	+58 14 37.0	20.312	1.930	3.308	0.8 ±0.4	3.1 ±0.3	0.13 ±0.01	
132	21 39 56.4	+58 13 47.7	17.783	1.584	2.274	1.3 ±0.4	2.5 ±0.2	0.33 ±0.01	
133	21 40 21.8	+58 14 45.6	20.447	1.749	3.312	0.7 ±0.5	3.6 ±0.5	0.13 ±0.01	

Table 5. Average age of the YSOs associated with the inside/outside regions of the BRCs.

BRC	Region	No. of stars	Mean age ± std dev (Myr)	Mean Av ± std dev (mag)
Only Hα stars				
BRC 2	On/Inside BR	11	1.0 ± 1.0	3.1 ± 1.4
	Outside BR	-	-	-
BRC 11	On/Inside BR	4	1.5 ± 1.1	2.4 ± 1.4
	Outside BR	5	2.1 ± 1.4	2.1 ± 1.4
BRC 13	On/Inside BR	3	0.6 ± 0.9	1.7 ± 0.9
	Outside BR	2	1.6 ± 0.9	1.7
BRC 14	On/Inside BR	13	1.0 ± 0.7	3.9 ± 1.8
	Outside BR	12	1.6 ± 0.7	3.0 ± 0.6
BRC 27	On/Inside BR	11	2.2 ± 1.1	2.3 ± 0.6
	Outside BR	12	2.2 ± 2.5	0.7 ± 0.7
BRC 38	On/Inside BR	6	2.1 ± 1.0	3.2 ± 1.1
	Outside BR	1	1.5	2.8
Hα and NIR excess stars				
BRC 2	On/Inside BR	13	1.0 ± 1.0	3.0 ± 1.4
	Outside BR	-	-	-
BRC 11	On/Inside BR	8	1.5 ± 0.8	2.3 ± 1.2
	Outside BR	6	2.1 ± 1.3	2.4 ± 1.5
BRC 13	On/Inside BR	3	0.6 ± 0.9	1.8 ± 0.9
	Outside BR	2	1.6 ± 0.8	1.7
BRC 14	On/Inside BR	15	1.1 ± 0.7	3.6 ± 1.9
	Outside BR	21	1.7 ± 0.8	2.0 ± 1.3
BRC 27	On/Inside BR	15	2.3 ± 1.2	2.7 ± 1.2
	Outside BR	14	1.9 ± 1.4	0.7 ± 0.7
BRC 38	On/Inside BR	7	2.1 ± 0.9	3.3 ± 1.0
	Outside BR	4	2.7 ± 0.9	1.4 ± 1.0

formation of new generation of stars at the peripheries of H II regions (see e.g. Elmegreen 1998), is quite common in the Galaxy. Some different triggering mechanisms may work in such regions. Briefly, the process which has been frequently supported by the observations is RDI, which takes place in small remnant clouds such as BRCs. The signature of star formation due to RDI is the presence of bright rims and embedded IR sources just inside the dense head. The collect-and-collapse model is another mechanism proposed by Elmegreen & Lada (1977). The signature of this process

are the presence of a collected, dense layer adjacent to the ionization front and the presence of massive condensations in it (e.g. Deharveng et al. 2003).

6.1 Small-Scale Sequential Star Formation

As for the S^4F hypothesis on the RDI star formation, there has been only qualitative evidence such as an asymmetric distribution of probable TTSs (Ogura et al. 2002) and of

properties of NIR excess stars (Matsuyanagi et al. 2006). Very recently Paper I (Ogura et al. 2007) have quantitatively verified the S^4F hypothesis by using BVI_c photometry of four BRCs. In the present study we follow the approach as given in Paper I. We have divided the YSOs ($H\alpha$ stars and NIR excess stars) associated with BRCs into two groups: those lying on/inside and outside of the rims (see Fig. A1). Mean ages and mean A_V values have been calculated for these regions. Some of the stars in Table 4 show ages older than 5 Myr. Since the ages of the associated ionizing sources of BRCs studied here have maximum ages of 4-5 Myr, therefore the TTSs having ages greater than this can not be expected as products of triggered star formation. We suspect that they may have formed spontaneously in the original molecular cloud prior to the formation of the HII region (see Sect. 6.3). Some of them may be background stars; larger distances make them look older in the CM diagram. So while calculating the mean ages we have not included those stars. The results are given in Table 5, which shows that in almost all the BRCs the YSOs lying on/inside the rim are younger than those located outside it, whereas the mean A_V is higher on/inside the bright rim than outside it. The only exception for the mean age is BRC 27.

The above results are exactly the same as those obtained in Paper I. Therefore, the present results further confirm the S^4F hypothesis. As in Paper I, we again find a big scatter in the stellar ages for each region of all BRCs in spite of a clear trend of the mean ages. Possible reasons for the scatter include photometric errors, errors in extinction correction, light variation of young stars, their proper motions, binarity of the stars, etc. Photometric errors and light variation as big as 0.5 mag would affect stellar ages by ~ 0.25 dex, so they do not seem to be the major reason for the scatter. As to the extinction correction, it probably does not affect the results much again, because in the $V_0, (V - I_c)_0$ CMD the isochrones are nearly parallel to the reddening vector. The adopted evolutionary models and distances of the BRCs causes systematic shifts in ages of the stars, but will not introduce scatters. As discussed in Paper I, we speculate that the proper motions of the newly born stars may probably be the main cause of the scatter.

Since stars inside the rim are often deeply embedded, mid-infrared (MIR) observations through the *Spitzer Space Telescope* can provide a deeper insight into the embedded YSOs. YSOs occupy distinct regions in the IRAC colour plane; this makes MIR colour- colour diagram a very useful tool for the classification of YSOs. Whitney et al. (2003) and Allen et al. (2004) presented independent model predictions for IRAC colours of various classes of YSOs. Fig. 3 presents $[5.8]-[8.0]$ versus $[3.6]-[4.5]$ colour-colour diagrams for the sources lying in the BRCs 2, 27 and 13/14 regions. The sources within the box represents the location of Class II objects (Megeath et al. 2004, Allen et al. 2004). The sources located around $[5.8]-[8.0]=0$ and $[3.6]-[4.5]=0$ are foreground/background stars, as well as diskless PMS stars (Class III objects). Sources with $[3.6]-[4.5] \geq 0.8$ and/or $[5.8]-[8.0] \geq 1.1$ have colours similar to those derived from models of protostellar objects with in-falling dusty envelopes (Allen et al. 2004). These are Class 0/I sources.

On the basis of the initial results from the *Spitzer* young cluster survey, Megeath et al. (2004) found a cluster of young stars near the edge of BRC 2 along with a group of Class I

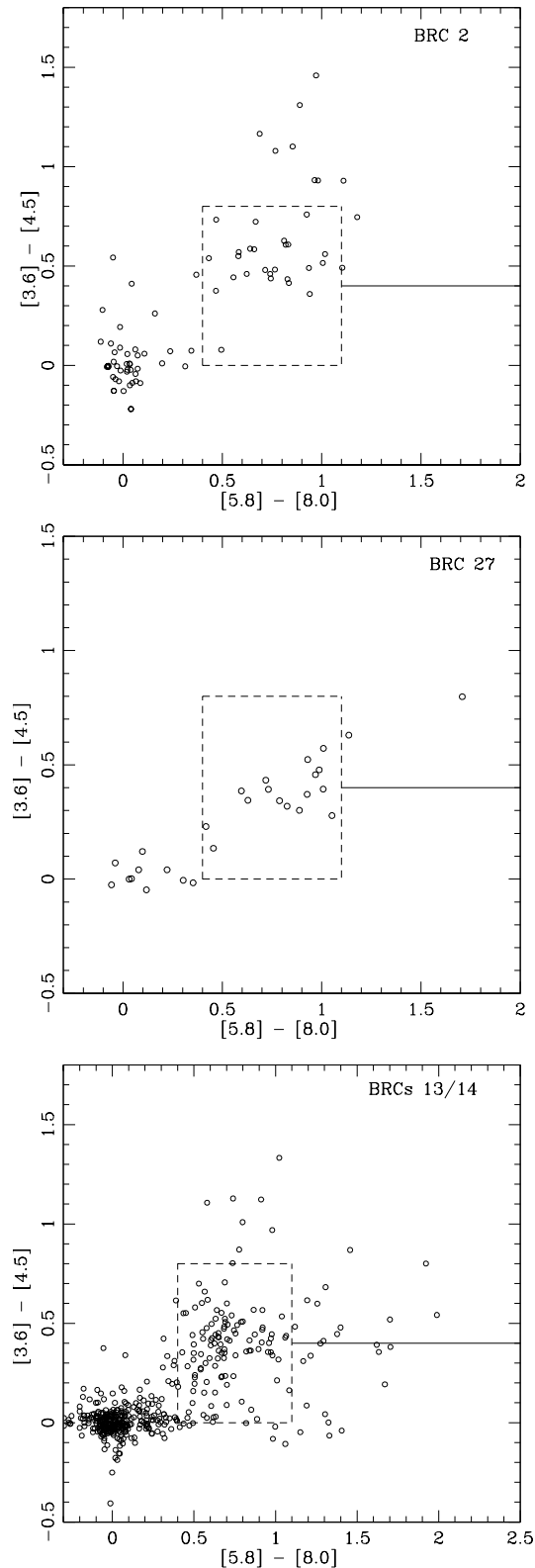


Figure 3. IRAC colour-colour diagrams for YSOs in BRCs 2, 27 and 13/14. The sources lying within the box are Class II sources. The sources located around $[5.8]-[8.0] \sim 0$ and $[3.6]-[4.5] \sim 0$ are the field/ Class III stars. Sources with $[3.6]-[4.5] \geq 0.8$ and/or $[5.8]-[8.0] \geq 0.8$ represent Class 0/I sources. The horizontal continuous line shows the adopted division between Class I and Class I/II sources (see Megeath et al. 2004).

Table 6. IRAC photometric magnitudes of the disk bearing candidates in BRCs 2, 27 and 13/14. The complete table is available in electronic form only.

RA (J2000)	DEC (J2000)	[3.6]	e[3.6]	[4.5]	e[4.5]	[5.8]	e[4.5]	[8.0]	e[8.0]	IRAC type
BRC 2										
00 04 14.69	+68 32 49.8	11.899	0.033	10.97	0.03	10.095	0.052	8.985	0.028	0/I
00 03 57.27	+68 33 24.4	12.231	0.038	11.74	0.042	11.100	0.087	9.996	0.075	0/I
00 04 03.83	+68 32 49.6	13.316	0.064	12.57	0.062	11.749	0.123	10.57	0.117	0/I

sources at the northern apex of the cluster. Table 6 summarizes the IRAC magnitudes of the disk bearing candidates of BRCs 2, 27 and 13/14, which is available in electronic form only. We reproduce the spatial distribution of the Class I and Class II sources in the BRCs 2 and 27 regions in Fig. 4. The upper panel for BRC 2 shows that the majority of the Class I sources are preferentially located away from the ionization sources (which lies downward in Fig. 4) as compared to the Class II sources. If we divide the BRC into two regions at $Dec. \geq 60^{\circ}34'.5$, the fraction of Class 0/I sources in the northern region (which is away from the ionizing source) is found to be 0.55 (6 Class 0/I and 5 Class II sources), which is significantly higher than that (0.16, 3 Class 0/I and 16 Class II sources) in the southern region (towards the ionizing source). This distribution further manifests a small scale age sequence in the BRC 2 region.

In the cases of BRCs 13 and 14, Allen et al. (2005) reported that the Class I protostars are tightly clustered on the edge of the molecular clouds, coincident with the interface of the ionized and molecular gas, whereas the Class II stars are more widely distributed. The distribution of YSOs detected using the IRAC data is reproduced in Fig. 5, where again Class 0/I sources are found concentrated inside the BRCs, which is in accordance with the S^4F hypothesis. In the IC 1396N = BRC 38 region, Getman et al. (2007) found an elongated spatial distribution of YSOs with the youngest stars (Class 0/I) deeply embedded inside the cloud and relatively older stars aligned toward the exciting star, which again supports propagation of small-scale triggered star formation in that region.

6.2 Indication of Global Triggered Star Formation

BRCs are considered to be a sort of remnants originated from dense part (cores) in an inhomogeneous giant molecular cloud. So, if the original cloud was big, the resultant BRC could have undergone a series of RDI events, leaving an elongated distribution of young stars; the distribution of such YSOs and its morphological details could be used to probe the star formation history in the OB association. With this expectation we have searched for NIR excess stars by using 2MASS PSC in the whole HII regions where the studied BRCs are located. Figs. A2 to A5 show spatial distribution of NIR excess stars in the IC 1848W, IC 1848E, CMaR1 and IC 1396 regions which contain BRCs 11NE, 13/14, 27 and 38 respectively. These figures are available in electronic form only. Figures 6 to 8 show radial variation of $\Delta(H - K)$ and A_V , for the stars located within the strip shown in Figs. A2 to A4. The NIR data along with $\Delta(H - K)$ and A_V values are given in Table 7, which is available in electronic form only.

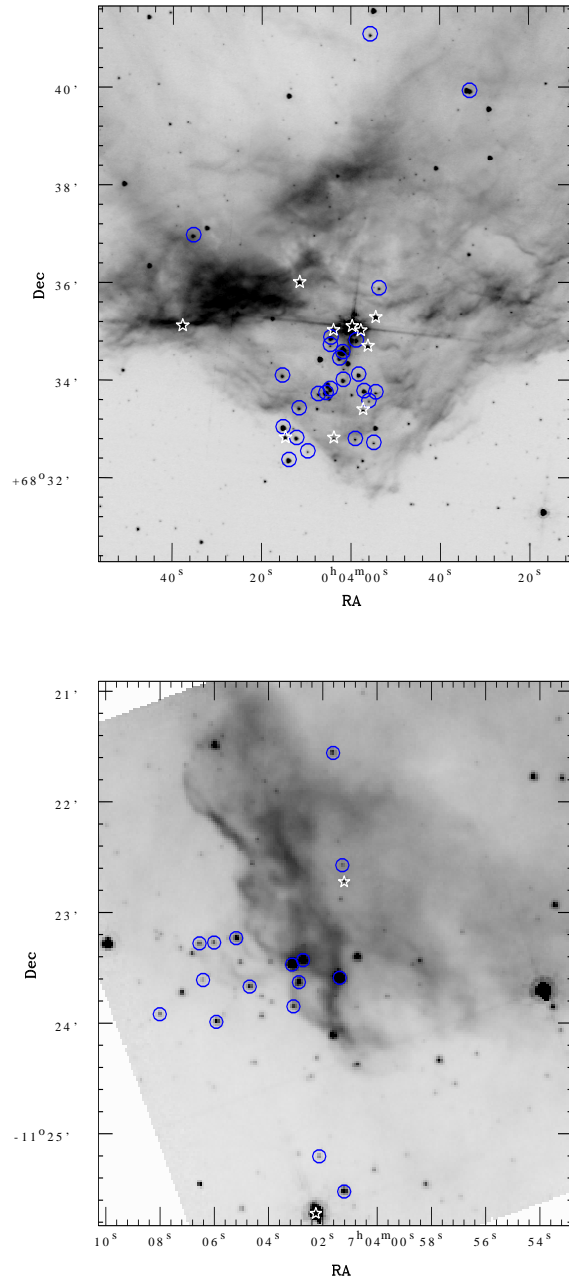
**Figure 4.** Spatial distribution of Class 0/I sources (star symbols) and Class II sources (open circles) in the BRC 2 (upper panel) and BRC 27 (lower panel) regions.

Table 7. J , H and K magnitudes of the sources used in the analysis (cf. sec. 6.2). The complete table is available in electronic form only.

RA (J2000)	DEC (J2000)	2MASS Name	$J \pm eJ$ (mag)	$H \pm eH$ (mag)	$K \pm eK$ (mag)	Q flag	C flag	A_V (mag)	$\Delta(H - K)$ (mag)	2MASS/Matsuyanagi et al. 2006(M06)
IC 1848W										
02 51 12.63	+60 24 00.1	02511262+6024000	13.719 ± 0.050	12.912 ± 0.051	12.361 ± 0.035	AAA	000	0.00	0.05	2MASS
02 51 24.86	+60 21 40.2	02512485+6021402	14.305 ± 0.038	13.545 ± 0.043	13.017 ± 0.031	AAA	000	0.00	0.05	2MASS
02 51 12.27	+60 25 51.3	02511226+6025512	15.955 ± 0.086	15.189 ± 0.103	14.630 ± 0.099	AAA	c00	0.00	0.08	2MASS

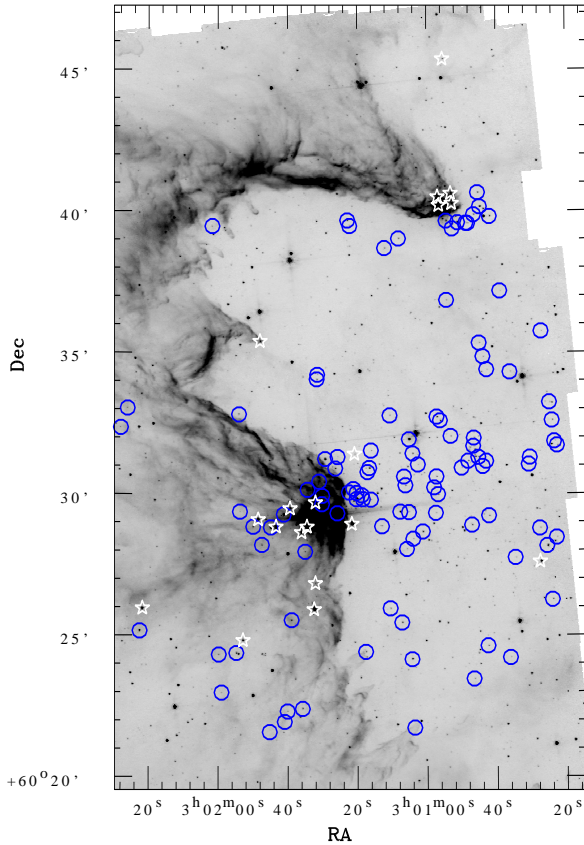
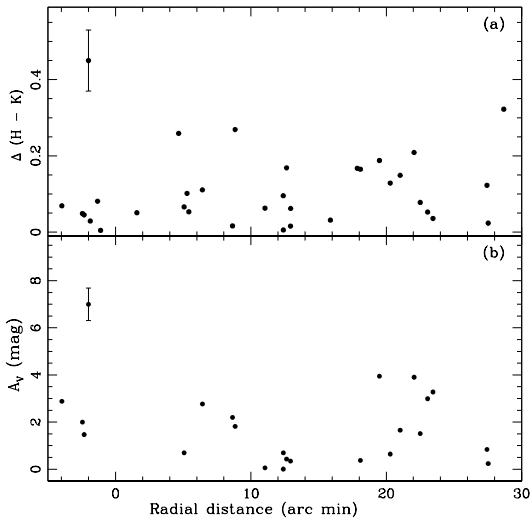

Figure 5. Spatial distribution of Class 0/I sources (star symbols) and Class II sources (open circles) in the BRCs 13 and 14 region identified in the *Spitzer/IRAC* data.

Fig. A2 shows that the NIR excess stars are aligned loosely towards the direction of BRC 11NE from the cluster IC 1848W which contains the ionizing sources (HD 17505, O6 V; HD 17520, O9V) of the HII region. A very recent study (while the present study was in the reviewing process) based on *Spitzer* observations by Koenig et al. (2008) also shows a nice alignment of Class II stars towards the direction of the BRC 11NE region from the ionizing source(s) (see their Fig. 10). Figs. 6a and 6b show radial variation of $\Delta(H - K)$ and A_V , for the stars in the BRC 11NE region located within the strip shown in Fig. A2, as a function of radial distance from HD 17505. $\Delta(H - K)$ is defined as the horizontal displacement from the middle reddening vector (see Fig. 1). The distribution of the NIR excess $\Delta(H - K)$ values shows an increasing trend as we move towards the BRC 11NE region. For the whole sample shown in Fig. 6a, the Kendall's tau test gives a positive correlation at a confidence level of about 85%. The two extreme points at radial distance $\sim 28'$ have small $\Delta(H - K)$ values with small A_V


Figure 6. Variation of (a) NIR excess $\Delta(H-K)$ and (b) A_V for the stars within the strip shown in Fig. A2 as a function of distance from HD 17505 toward BRC 11 region. Average error bar is shown at the upper-left corner of the plot.

(0.24 and 0.84) values. We presume that these sources are not embedded inside the rim and lying on the outer region of the cloud. The two stars at radial distance $\sim 5'$ and $\sim 9'$ shows relatively higher value of $\Delta(H - K)$ in comparison to nearby stars. Exclusion of these four points gives a probability of $\sim 97\%$ for a positive correlation between radial distance and $\Delta(H - K)$. Table 8 summarizes the results of the correlation analysis using the Kendall's tau test.

On the basis of the pressure of the ionized boundary layer (IBL) and that of the molecular cloud, Thompson et al. (2004) have concluded that the cloud is in pressure balance with the exterior ionized gas and photo ionization induced shocks are propagating in the cloud. They also concluded that overall morphology of the cloud is similar to that predicted by RDI models (Bertoldi 1989, Lefloch & Lazareff 1994). They have also estimated the duration over which the BRC 11NE region might have been exposed to the UV flux. Assuming that the rims are located at a distance of ~ 22 pc from the ionizing sources, an ionization front expanding into a medium of homogeneous density at a speed of 11.4 km/s will take about 1.5 Myr to reach the rims. The mean age of the YSOs ($H\alpha$ stars and NIR excess stars) associated with BRC 11NE (both inside and outside the bright rim) is found from Table 4 to be 1.7 ± 1.0 Myr. Thus the sum of these two values yields a time scale of ~ 3.2 Myr, which is comparable to the MS lifetime (~ 4.0 Myr) of HD 17505 (Lang 1992, Schaller et al. 1992). The above facts seems to support the triggered star formation scenario in the IC 1848W region.

Figure A3 shows that the distribution of the NIR excess stars in the IC 1848E region. We see they are aligned

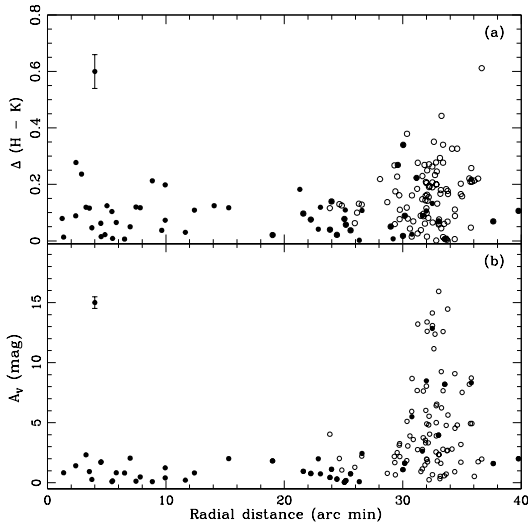


Figure 7. Variation of (a) NIR excess $\Delta(H-K)$ and (b) A_V as a function of the distance from HD18326 toward BRC 14. Filled and open circles represents the data taken from the 2MASS catalogue and Matsuyanagi et al. (2006), respectively. Average error bar is shown at the upper-left corner of the plot.

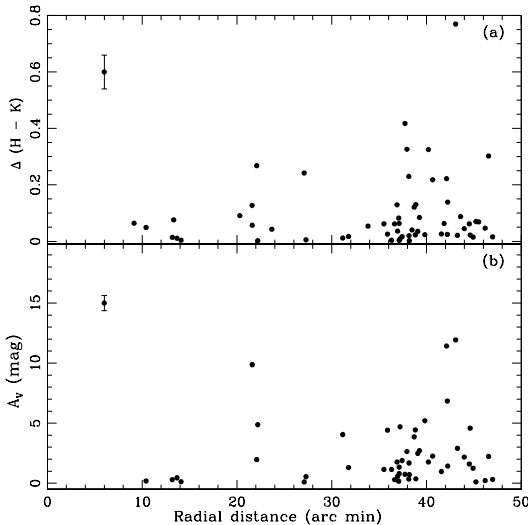


Figure 8. Variation of (a) NIR excess $\Delta(H-K)$ and (b) A_V for the stars within the strip shown in Fig. A4 as a function of distance from the probable ionizing source (HD 53974) of the CMaR1 region. Average error bar is shown at the upper-left corner of the plot.

beautifully from the vicinity of the O7 star HD 18326 to the direction of BRC 14. A more impressive alignment of the Class II sources can be seen in Fig. 7 of Koenig et al. (2008). This spatial distribution of NIR excess stars resembles that in NGC 1893, where a similar nice distribution of NIR excess stars is noticed from the centre of the cluster containing several OB stars to the direction of the cometary globules Sim 129 and 130 (see Fig. 22 of Sharma et al. 2007). In the case of NGC 1893 evidence for triggered star formation due to RDI is also found. In Fig. 7a (upper panel) we plot the amount of NIR excess $\Delta(H-K)$ for the stars shown in Fig. A3 as a function of radial distance from the center of the cluster. Fig. 7a manifests an increase in NIR excess near

BRC 14. A similar trend is noticed for the spatial distribution of A_V (Fig. 7b). Kendall's tau test yields a positive correlation for the radial variation of $\Delta(H-K)$ and A_V at a confidence level of better than 99.9%. As discussed in Matsuyanagi et al. (2006), these features indicate that stars located near BRC 14 should be younger than the rest of the stars.

In Fig. A3 a loose clustering is also clearly visible around HD 18326. To our knowledge this clustering has not been designated so far as a known cluster¹. $J/(J-H)$ CM diagram of the cluster region yields an age of ~ 2 Myr. This cluster will be studied in detail in a forthcoming paper. On the other hand, the mean age of the YSOs associated with BRCs 13 and 14 (again, both inside and outside of the rims) is derived from Table 4 to be 1.0 ± 0.9 Myr and 1.5 ± 0.9 Myr, respectively, which are younger than the age of the cluster. Recently Nakano et al. (2008) reached the same conclusion, obtaining the ages of 4 Myr and 1 Myr for a groups of H α emission stars around HD 18326 and that near eastern edge of the HII region, respectively. This again indicates that the star formation in the BRCs 13/14 region is triggered by the O star in the cluster region. Thus all the above mentioned evidences clearly support a series of RDI processes which took place in the past starting from the vicinity of the O star.

The spatial distribution of the NIR excess stars in the BRC 27 region is shown in Fig. A4. Assuming that B0.5IV (HD 53974; marked as '2') and B1V (HD 54025; marked as '1') stars are the ionizing sources for the BRC 27 region, the $\Delta(H-K)$ and A_V distribution for the sources lying within the strip marked in Fig. A4 as a function of radial distance from HD 54025 is shown in Fig. 8, which indicates relatively higher NIR excess and A_V near the BRC 27 region. The Kendall's tau test for the entire sample indicates a positive correlation between radial distance and $\Delta(H-K)$ and A_V at a confidence level of $\sim 80\%$ and $\sim 95\%$, respectively. The sources having radial distance $> 43'$ show small value of A_V as well as $\Delta(H-K)$ as compared to the sources lying around $40' - 41'$. We presume that these sources are not embedded inside the rim and are lying on the outer periphery of the cloud. Exclusion of these points gives a probability of $\sim 98\%$ or better and 99.9% for a positive correlation between radial distance and $\Delta(H-K)$; and A_V , respectively. If the B1V/B0.5 IV star(s) is (are) actually the ionizing source(s) for the region, the maximum MS life-time of the star(s) is ~ 10 Myr (Lang 1992, Schaller et al. 1992), whereas the mean age of the YSOs associated with BRC 27 is estimated as 2.1 ± 1.3 Myr, which is not in contradiction with that star formation in the BRC 27 region may be initiated by the UV-radiation from these star(s).

Sicilia-Aguilar et al. (2004) have shown that in the case of the Tr 37/ IC 1396 Globule region, CTTs are found to be aligned towards the direction of IC 1396 Globule from the ionizing source, HD 206267 (O6). Sicilia-Aguilar et al. (2005) found that most of the younger (~ 1 Myr) members appear to lie near or within the IC 1396 Globule. They concluded that it can be indicative of the triggered star formation. Fig. A5 shows distribution of NIR excess stars in the Tr 37/IC 1396

¹ In a very recent study based on *Spitzer* observations, Koenig et al. (2008) have also identified this cluster.

Table 8. Correlation between radial distance and $\Delta(H-K)$, A_V . The probability P(0) indicates that no correlation is found with the generalized non-parametric Kendall's tau statistics.

Radial distance from the ionizing source (arc min)	P (0) $\Delta(H-K)$	P (0) A_V	comment
BRC 11			
5 - 30	0.150	-	
5 - 30	0.026	-	Excluding Outliers (see text)
BRC 14			
0 - 40	< 0.00	< 0.00	
BRC 27			
0 - 48	0.230	0.04	
0 - 43	0.025	0.001	(see text)

Globule/BRC 38 region, where they seem to align loosely towards the direction of IC 1396 Globule and BRC 38. Their radial distribution of NIR excess $\Delta(H-K)$ and A_V does not show any trend, however. By using the ages of the YSOs near IC 1396 Globule given by Sicilia-Aguilar et al. (2005) we obtained their mean age of $\sim 1.8 \pm 1.1$ Myr, whereas for the YSOs near BRC 38 the mean age is estimated from Table 4 to be $\sim 2.2 \pm 0.9$ Myr. The upper main-sequence turn off age of Tr 37 is found to be ~ 3 Myr (Contreras et al. 2002). Thus the aligned distribution of YSOs from the ionizing source HD 206267 towards IC 1396 Globule and BRC 38 and their younger age as compared to the central cluster Tr 37 suggest a triggered star formation scenario in the region.

We conclude that the global distribution of YSOs, their radial distribution of the amount of NIR excess $\Delta(H-K)$ as well as of A_V in each HII region studied here clearly show evidence that a series of RDI processes proceeded in the past from near the central O star(s) towards the peripheries of the HII region.

6.3 Star Formation inside ‘A’-Type BRCs

The *Spitzer* IRAC data on BRC 2, BRC 13 and BRC 14 manifest that the Class 0/I sources are concentrated inside the rim. The SCUBA imaging survey of submillimeter continuum emission from BRCs by Morgan et al. (2008) has shown that the embedded cores are likely to contain Class 0 protostars. On the basis of combination of the observed submillimeter flux excess and high dust temperature they concluded that star formation may be on-going within the BRCs. They have further concluded that the majority of the sources have $L_{bol} > 10L_{\odot}$, indicating that the sources are intermediate to high-mass stars. Some of the higher luminosity sources (e.g. in BRCs 13 and 14) may be proto-clusters. The *Spitzer* IRAC data manifest that in fact these two BRCs host a proto-cluster (cf. Fig. 6).

Morgan et al. (2008) did not find evidence for interaction of the external ionization field with the star formation inside ‘A’ type BRCs (for the morphological types of BRCs we refer to SFO91) and concluded that the star formation in these clouds is not subjected to the RDI process. The present work includes four BRCs of the ‘A’ type, namely, BRCs 2,

14, 27 and 38 (as for BRC 38, see Sect. 8) and provides strong evidence for star formation due to RDI occurring in BRCs, however. As we have seen in Sect. 6.1, BRCs 2, 14 and 38 show such age gradients that stars located on/inside the rim are younger than those located outside it, i.e., toward the ionizing source, evidencing the most recent RDI phenomenon. In addition, our results in Sect. 6.2 as well as recent study based on *Spitzer* observations by Koenig et al. (2008) manifest a nice, global alignment of NIR excess stars in IC 1848E from the O7 star HD 18326 to BRCs 13 and 14. The spatial distribution of H α emission stars found by Nakano et al. (2008) also revealed a similar alignment. Thus the ages of the YSOs and their spatial distribution in the region clearly support a series of RDI processes which have been taking place in the past until very recently. These results do not support the notion of Morgan et al. (2008) that star formation in/around ‘A’-type BRCs is not subjected to the RDI triggering process.

7 EVOLUTION OF H α EW AND DISK OF T-TAURI STARS

H α emission and IR excess are important signatures of young PMS stars. These signatures in CTTSs indicate the existence of a well-developed circumstellar disk actively interacting with the central star. Strong H α emission (equivalent width EW $> 10\text{\AA}$) in CTTSs is attributed to the magnetospheric accretion of the innermost disk matter onto the central star (Hartmann et al. 1994; Edwards et al. 1994; Muzerolle et al. 2001 and references therein). On the other hand the weak H α emission (EW $< 10\text{\AA}$) in weak-line TTSSs (WTTSSs), which lack disks (or, at least inner disks), is believed to originate from their chromospheric activity (e.g., Walter 1988; Martin 1998). In 1990s a large number of WTTSSs were found in and over wide areas around T associations by X-ray surveys with ROSAT, which aroused active studies on the nature of the so-called dispersed WTTSSs. For a detailed discussions on this topic we refer to Caillault et al. (1998). As for the relation of the WTTSS to the CTTS, the ‘‘standard model’’ (Kenyon and Hartmann 1995) postulates that the latter evolves to the former by losing the circumstellar disk (or, at least its inner part). Actually analysis of the age distribution derived from the HR diagram of, e.g., the Taurus region indicated that the WTTSSs are systematically older than the CTTSs, but the statistical significance was low (Kenyon and Hartmann 1995; Hartmann 2001; Armitage et al. 2003).

On the other hand, there also have been many observations which claimed that the CTTS and the WTTSS are coeval and have indistinguishable stellar properties (e.g., Walter et al. 1988; Lawson et al. 1996; Gras-Velazquez and Ray 2005). From the analyses of the HR diagram of the CTTSs and WTTSSs in Chamaeleon I, Lawson et al. (1996) concluded that some stars may be born even almost diskless or lose the disk at very early stages (age < 1 Myr). However, in order to explain the co-existence and approximate coevality of CTTSs and WTTSSs in a star forming region, it is usually postulated that YSOs display a wide range of disk masses and their accretion activity and/or the dispersal of the disk takes place in a correspondingly wide range of time-scales (Bertout et al. 2007; Furlan et al. 2006). Based on L-

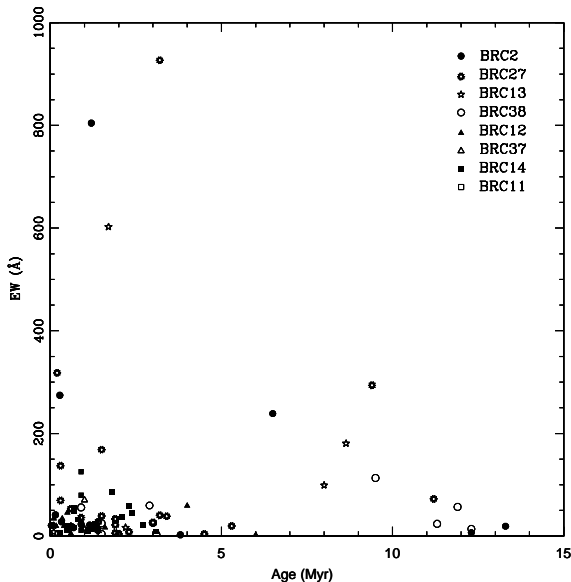


Figure 9. EWs of $H\alpha$ emission stars in our sample as a function of stellar ages.

band surveys of clusters of various ages, Haisch et al. (2001) reached the quantitative conclusion that the disk fraction is initially very high ($\geq 80\%$) and that one half the stars lose their disks in ~ 3 Myr and almost all in ~ 6 Myr. Armitage et al. (2003) obtained similar results that around 30% of stars lose their disks within 1 Myr, while the remainder have disk lifetimes that are typically in the 1 - 10 Myr range. Recently, Bertout et al. (2007), by using new parallaxes for CTTS and WTTS in the Taurus-Auriga T association, concluded that their observed age and mass distribution can be explained by assuming that a CTTS evolves into a WTTS when the disk is fully accreted by the star.

In the present work we have derived the ages of 93 $H\alpha$ emission stars, hence we can study the evolution of the $H\alpha$ emission activity in TTSs. The advantage of our sample in addressing this issue is that the stars are spatially, i.e., three-dimensionally, very close to each other, so there should be no problem of the distance difference, contrary to the extended T associations. The $H\alpha$ EWs are taken from Ogura et al. (2002); however the values reported as EWs in their Table 5 are values in pixels. To convert these values into \AA we multiply the reported values by a factor of 3.8 (see Ikeda et al. 2008).

In Fig. 9 we plot the EWs of $H\alpha$ emission stars as a function of age to explore possible evolutionary trends. Although, the dispersion around younger side is quite large, still in general there seems to be a decreasing trend in EW with the age. Here it is worthwhile to mention that a rather similar trend in the EWs of $H\alpha$ emission line of H Ae/Be stars is reported by Manoj et al. (2006). The distribution of EWs in Fig. 9 indicates that the accretion activity in the TTSs associated with BRCs drops substantially by 5 Myr. In Fig. 9, there seems to be a small group of $H\alpha$ emission stars having far larger ages (≥ 5 Myr) and a relatively elevated level of EWs. The masses of these stars lie in the range $0.6 \geq M/M_{\odot} \geq 1.9$, whereas the majority of the YSOs having age ≤ 5 Myr have masses in the range $0.1 \geq M/M_{\odot} \geq 1.2$. If we take their ages at their face val-

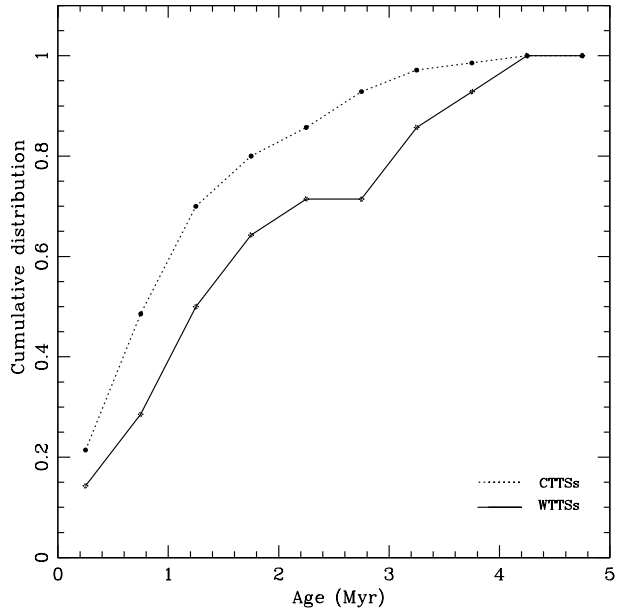


Figure 10. Cumulative distributions of CTTSs and WTTSs in our sample as a function of stellar age.

ues, they presumably are not products of triggering. Since the ages of the ionizing sources of BRCs studied here have maximum age of 4-5 Myr, stars having ages greater than ~ 5 Myr can not be expected as results of triggered star formation, but must have formed spontaneously prior to the formation of the HII region. The stars with ages ≥ 5 Myr seems to born with large disk masses and spent a substantial part, say, half of their ages unexposed to UV radiation from O stars, the long lifetime of their accretion activity may be understood. Johnstone et al. (2004) have reported that the far-UV radiation from nearby massive star(s) may cause photo-evaporation of YSO disks resulting in short ($\sim 10^6$ yr) disk lifetimes. However, Fig. A1, where these stars are marked with crosses, shows that they are located both inside and outside the bright rims mixed with $H\alpha$ stars of younger ages. So their origin remains a mystery. But in the case of BRC 38, which contributes four to this group of altogether eleven stars, Getman et al. (2007) recognized, apart from young stars associated with the BRC, an older population of PMS stars dispersed in IC 1396. We suspect the above four stars may belong to this population and formed in the original molecular cloud prior to the formation of HD 206267. In Fig. A1 they look concentrated along the bright rim, but note that the $H\alpha$ survey by Ogura et al. (2002) is limited down to +58 13 35, which is only a few arcmin south of the bright rim. Here it is worthwhile to mention that in the case of cluster Tr 37 (age 1-5 Myr), Sicilia-Aguliar et al. (2005) have found a few stars having age > 5 Myr. They pointed out that in some clusters intermediate-mass stars seem older than low-mass stars and this effect seems to be related to a problem defining the birth line for intermediate-mass stars (Hartmann 2003).

Figure 10 shows the cumulative distribution of CTTSs ($EW \geq 10\text{\AA}$) and WTTSs ($EW < 10\text{\AA}$) (for stars having age ≤ 5 Myr) as a function of age. Fig. 10 manifests that CTTSs are relatively younger than WTTSs. A Kolmogorov-Smirnov test confirms the statement that the cumulative

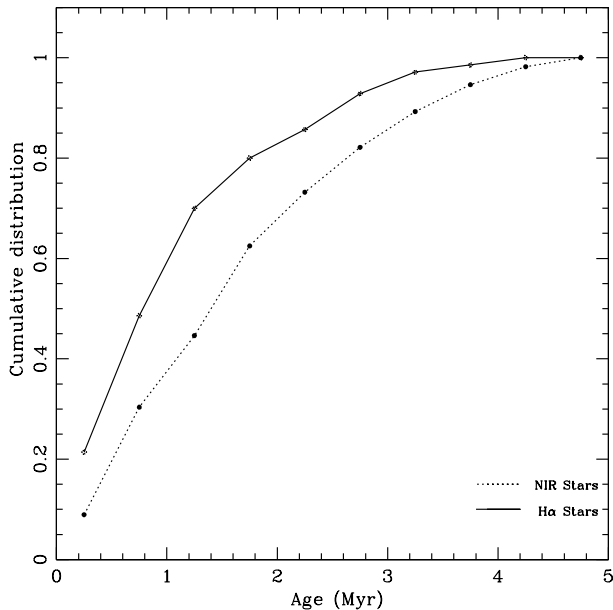


Figure 11. Cumulative distributions of H α emission and NIR excess stars in our sample as a function of stellar age.

distributions of CTTSs and WTTSs are different at a mean confidence level of $\sim 70\%$ with minimum and maximum confidence level (obtained using the Monte Carlo simulations) of $\sim 55\%$ and $\sim 90\%$, respectively. This result is in agreement with that of Bertout et al. (2007) for the Taurus-Auriga T-association, that WTTSs are older than CTTSs and CTTSs evolve into WTTSs. In Fig. 11 we plot cumulative age distribution of H α emission stars ($EW \geq 10\text{\AA}$) and of NIR excess stars. Fig. 11, at a mean confidence level of $\sim 98\%$ (with a minimum and maximum confidence level of $\sim 92\%$ and $\sim 99.4\%$) indicates that YSOs exhibit NIR excess for a relatively longer time as compared to accretion activity. Although our sample is small and the age span is very short, the obtained CTTS fraction (from Tables 3 and 4) in BRCs seems to follow the trend of TTSs in the Taurus region as given by Armitage et al. (2003).

8 MASS FUNCTION OF BRC AGGREGATES

The initial mass function (IMF) is an important tool to study the star formation process. Morgan et al. (2008), using SCUBA observations, have estimated the masses of 47 dense cores within the heads of 44 BRCs. They concluded that the slope of the mass function of these cores is significantly shallower than that of the Salpeter mass function. They also concluded that it depends on the morphological type of BRCs (for the morphological description of BRCs we refer to SFO91): ‘A’ type BRCs appear to follow the mass spectrum of the clumps in the Orion B molecular cloud, whereas the BRCs of the ‘B’ and ‘C’ types have a significantly shallower mass function.

It would be worthwhile to compare the mass function of protostars given by Morgan et al. (2008) with that of BRC aggregates. In Fig. 12 we plot cumulative mass function (CMF) of the YSOs in 7 BRCs, namely BRCs 2, 11NE, 12, 13, 14, 27 and 38, in the mass range of $0.2 \leq M/M_{\odot} \leq 1.2$.

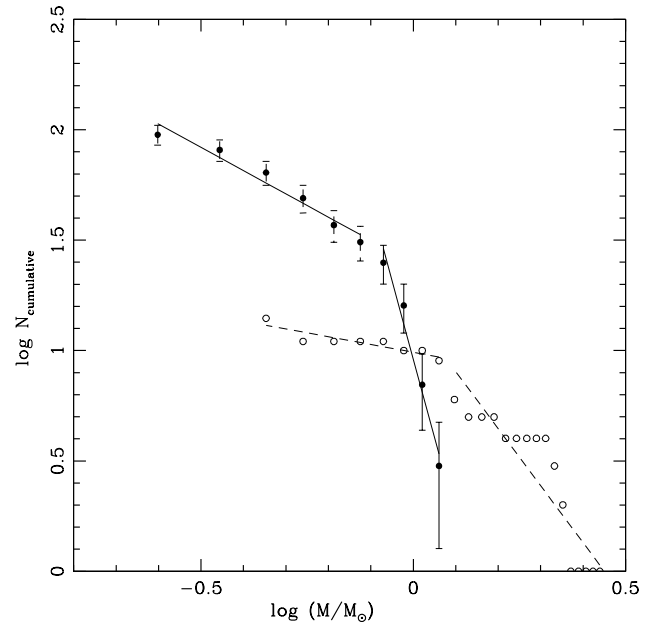


Figure 12. Cumulative mass function (CMF) of YSOs in the 7 BRCs (filled circles). Error bars represent $\pm\sqrt{N}$ errors. Open circles represent the CMF for the cores by Morgan et al. (2008).

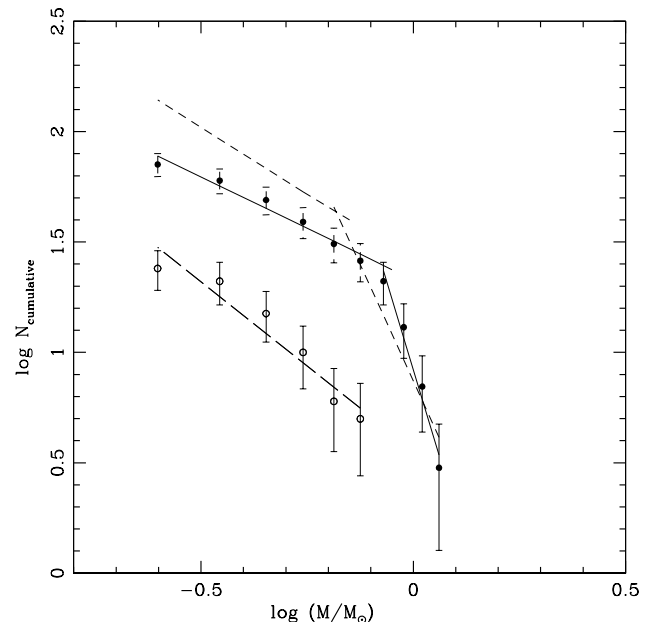


Figure 13. Cumulative mass function (CMF) of the ‘A’ type (filled circles) and ‘B/C’ type BRCs (open circles). Error bars represent $\pm\sqrt{N}$ errors. The CMF for the standard MF is shown by short dashed lines (see the text).

Here we have supplemented the present data with the data of BRC 12, taken from Paper I, because among the present sample of BRCs there are fewer number of BRCs of type ‘B’ than those of type ‘A’. The CMF of the dense cores by Morgan et al. (2008) is also plotted for comparison.

It is interesting to notice that both CMFs show a roughly similar shape with a break in power law. Obviously a detailed comparison manifests differences. In the case of the YSOs we find a break in the slope of the CMF at $\sim 0.8 M_{\odot}$.

In the mass range $0.8 \leq M/M_{\odot} \leq 1.2$ the slope of the CMF is -7.1 ± 0.9 and it becomes shallower (-1.0 ± 0.1) for masses $0.2 \leq M/M_{\odot} \leq 0.8$, whereas the CMF of the cores can be represented by a power law with a shallower slope of -0.4 ± 0.1 in the mass range $0.4 \leq M/M_{\odot} \leq 1.2$. The core CMF becomes steeper for masses $\geq 1.2 M_{\odot}$ (slope $= -2.6 \pm 0.3$). Morgan et al. (2008) have reported that their sample is complete down to $0.5 M_{\odot}$. Our sample toward lower mass may be affected by incompleteness, however the correction due to incompleteness will further steepen the CMF slope of the YSOs. The shallower CMF slopes in the case of dense cores than those for YSOs indicates that the star formation in the next sequence/ generation favours formation of relatively massive stars.

If the star formation within the BRCs depends on morphology of the clouds, as suggested by Morgan et al. (2008), it would be interesting to study the CMF of YSOs by separating the target BRCs on the basis of the morphology of BRCs. Here we assign type A to BRC 38 rather than type B given in SFO91. BRC 11NE, which is not included in SFO91, is classified as type B. In Fig. 13 we plot the CMFs of the YSOs in 4 ‘A’ type BRCs, namely BRCs 2, 14, 27 and 38, and of those in 3 ‘B/C’ type BRCs, namely BRCs 11NE, 12 and 13. In the YSO mass range $0.2 \leq M/M_{\odot} \leq 0.8$ the slope of the CMF for the ‘B/C’ type BRCs is found to be -1.5 ± 0.2 which is steeper than that (-0.9 ± 0.1) obtained for ‘A’ type BRCs. This is in contradiction with the results reported by Morgan et al. (2008). They reported a shallower mass function slope for ‘B/C’ type BRCs in comparison to that of ‘A’ type BRCs (see their Figure 11); however a close inspection of their figure 11 manifests that in the mass range $0.5 \leq M/M_{\odot} \leq 3.0$, the MF slope of the cores of ‘A’ type BRCs is definitely shallower than that for ‘B/C’ type BRCs. This suggests that ‘A’ type rims, in the mass range $0.4 \leq M/M_{\odot} \leq 1.2$, appear to follow a mass function that is more biased toward formation of relatively massive stars in comparison to that in case of ‘B’ and ‘C’ type BRCs.

In Fig. 13 we have also plotted the CMF generated for a sample aggregate having an average Galactic initial mass function, i.e., $\Gamma = -1.35$ for $0.6 \leq M/M_{\odot} \leq 1.2$, and $\Gamma = -0.3$ for $0.2 \leq M/M_{\odot} \leq 0.6$ (Kroupa 2001, 2002). The slope of the CMF in the mass range $0.2 \leq M/M_{\odot} \leq 0.6$ comes out to be $\sim 1.1 \pm 0.1$, which is close to the slope of the CMF (-0.9 ± 0.1) of the YSOs ($0.2 \leq M/M_{\odot} \leq 0.8$) in the ‘A’ type BRCs. Whereas, the CMF slope for YSOs in the ‘B/C’ type BRCs is significantly steeper (-1.5 ± 0.2) than the standard MF. This suggests that in the mass range $0.2 \leq M/M_{\odot} \leq 0.8$ the YSOs in ‘A’ type BRCs follow the standard form of MF, whereas aggregates in ‘B/C’ type BRCs is more biased towards relatively less massive objects. We have also estimated the effect of errors on estimation of mass function. The results are given in Table 9 which indicate an insignificant effect on the mass function slopes.

9 CONCLUSIONS

On the basis of the present optical and NIR analysis of six BRC aggregates we reached the following conclusions.

We estimated the ages of individual stars associated with BRCs from the reddening-corrected $V_0, (V - I_c)_0$ CM diagrams. By comparing the average ages of the stars

Table 9. Mass function of BRC aggregates. The maximum and minimum value of the slopes are estimated by propagating the random errors using the Monte Carlo simulations.

Mass Range (M_{\odot})	Mean value of the slope	Maximum value of the slope	Minimum value of the slope
All BRCs			
0.2 - 0.8	-0.97 ± 0.14	-0.99 ± 0.15	-0.95 ± 0.15
0.8 - 1.2	-7.08 ± 0.89	-8.17 ± 0.86	-6.40 ± 0.62
A-type BRCs			
0.2 - 0.8	-0.92 ± 0.09	-0.96 ± 0.10	-0.87 ± 0.11
0.8 - 1.2	-6.40 ± 0.78	-7.60 ± 0.74	-5.60 ± 0.55
B/C-type BRCs			
0.2 - 0.8	-1.53 ± 0.20	-1.63 ± 0.20	-1.20 ± 0.17

on/inside and outside the bright rim, we again found quantitative age gradients in almost all the studied BRCs (the only exception being BRC 27), although the number of the sample stars are small and their age scatters are large. The results are quite similar to the results reported in Paper I. In addition the youngest objects, obtained from *Spitzer* MIR data, are found to be deeply embedded inside the BRCs, supporting the above conclusion. These results further confirm S^4F hypothesis.

The distribution of NIR-excess stars in the studied HII regions indicates that they are aligned from the ionizing source to the BRC direction. The age indicators, viz., infrared excess ($\Delta(H - K)$) and A_V as well as the age itself of the YSOs manifest an age gradient toward the ionizing source. This global distribution indicates that a series of triggered star formation took place in the past from near the central O star(s) towards the peripheries of the HII region.

It is found that the EW of $H\alpha$ emission in TTSSs associated with the BRCs decreases with age. We found some $H\alpha$ emission stars that are significantly older than those TTSSs associated with the BRCs. They apparently must have formed spontaneously before the main star formation event which gave birth to the massive stars in the region; however their origin is not clear. We found that in general WTTSSs are older than CTTSs. It is also found that the fraction of CTTSs among the TTSSs associated with the BRCs is found to decrease with age, as found in Taurus region by Armitage et al. (2003). These facts are in accordance with the conclusion by Bertout et al. (2007) that CTTSs evolve into WTTSSs.

The CMF of ‘A’ type BRCs seems to follow a mass function similar to that found in young open clusters, whereas ‘B/C’ type BRCs have a significant steeper CMF, indicating that BRCs of the latter type tend to form relatively more low mass YSOs of the mass range $0.2 \leq M/M_{\odot} \leq 0.8$.

10 ACKNOWLEDGMENTS

We are thankful to the anonymous referee for the critical comments which improved the scientific contents and presentation of the paper. We are thankful to the TAC and staff of HCT for the time allotment and for their support during the observations, respectively. This publication makes use of

data from the Two Micron All Sky Survey (a joint project of the University of Massachusetts and the Infrared Processing and Analysis Center/ California Institute of Technology, funded by the National Aeronautics and Space Administration and the National Science Foundation), archival data obtained with the *Spitzer Space Telescope* (operated by the Jet Propulsion Laboratory, California Institute of Technology, under contract with the NASA). This study is a part of the DST (India) sponsored project and NC is thankful to DST for the support. NC also acknowledges the financial support provided by TIFR during her visit to TIFR. AKP and KO acknowledge the financial support received from DST (India) and JSPS (Japan).

REFERENCES

- Allen L.E., Calvet N., D'Alessio P. et al. 2004, ApJSS, 154, 363
- Allen L.E., Hora J.L., Megeath S.T., Deutsch L.K., Fazio G.G., Chavarria L., Dell R.W. 2005, IAUS, 227, 352
- Armitage P.J., Clarke C.J., Palla F. 2003, MNRAS, 342, 1139
- Bertoldi F., 1989, ApJ, 346, 735
- Bertout C., Siess L., Cabrit S. 2007, A&A, 473, L21
- Bessell M.S., & Brett J.M. 1988, PASP, 100, 1134
- Caillault J.P., Brice no C., Mart'in E.L., Palla F., Wichmann R. 1998, ASP Conf. Series, 154: Cool Stars, Stellar Systems and the Sun, 237
- Carpenter J.M., Heyer M.H., & Snell R.L. 2000, ApJS, 130, 381
- Cohen J.G., Frogel J.A., Persson S.E., & Ellias J.H. 1981, ApJ, 249, 481
- Contreras Maria E., Sicilia-Aguilar A., Muzerolle J., Calvet N., Berlind P., Hartmann L., 2002, ApJ, 124, 1585
- Cutri R.M., Skrutskie M.F., Van Dyk S. et al. 2003, Vizier Online Data Catalog, 2246, O
- Dale J.E., Binnell I.A., Whitworth A.P. 2007, MNRAS, 375, 1291
- Deharveng L., Zavagno A., Cruz-Gonzalez I., Salas L., Caplan, J., & Carrasco L. 1997, A&A, 317, 459
- Deharveng L., Zavagno A., Salas L., Porras A., Caplan J., & Cruz-Gonzalez I. 2003, A&A, 399, 1135
- De Vries C.H., Narayanan G., Snell R.L., 2002, ApJ, 577, 798
- Edwards S., Hartigan P., Ghandour L., & Andrulis C. 1994, AJ, 108, 1056
- Elmegreen B.G., & Lada C.J. 1977, ApJ, 214, 725
- Elmegreen B. G. 1998, ASP Conf. Series 148, 150, ed. Woodward C.E., Shull J.M., and Thronson H.A.
- Feinstein A., Vazquez R.A., Benvenuto O.G. 1986, A&A, 159, 223
- Furlan E., Hartmann L., Calvet N., D'Alessio P., Franco-Hernandez R., Forrest W.J., Watson D.M., Uchida K.I., Sargent B., Green J.D., Keller L.D., Herter T.L. 2006, ApJ, 165, 568
- Getman K.V., Feigelson E.D., Garmire G., Broos P., & Wang J. 2007, ApJ, 654, 316
- Girardi L., Bertelli G., Bressan A., Chiosi C., Groenewegen M.A.T., et al. 2002, A&A, 391, 195
- Gras-Vel'azquez A., & Ray T. P. 2005, A&A, 443, 541
- Haisch K.E., Lada E.A., & Lada C.J. 2001, AJ, 121, 2065
- Hartmann L., Hewett R., Calvet N. 1994, ApJ, 426, 669
- Hartmann L. 2001, AJ, 121, 1030
- Hartmann L. 2003, ApJ, 585, 398
- Herbst W., Assousa G.E. 1977, ApJ, 217, 473
- Hillenbrand L.A., Strom S.E., Vrba F.J., Keene J. 1992, ApJ, 397, 613
- Hillenbrand L.A. 2005, A Decade of Discovery: Planets Around Other Stars" STSci Symposium Series 19, ed. M. Livio, astro-ph/0511083
- Hosokawa T., & Inutsuka S.-I. 2005, ApJ, 623, 917
- Hosokawa T., & Inutsuka S.-I. 2006, ApJ, 646, 240
- Ikeda H., Sugitani, K., Watanabe M. et al. 2008, AJ, 135, 2323
- Johnstone D., Matsuyama I., McCarthy I. G., Font A. S., 2004, R. Mex. A&A, 22, 38
- Jose J., Pandey A.K., Ojha D.K., Ogura K., Chen W.P., Bhatt B.C., Ghosh S.K., Mito H., Maheswar G., Sharma S. 2008, MNRAS, 384, 1675
- Karr J.L., Martin P.G. 2003, ApJ 595, 900
- Kenyon S., & Hartmann L. 1995, ApJS, 101, 117
- Kessel-Deynet O., & Burkert A. 2003, MNRAS, 338, 545
- Koenig X. P., Allen L. E., Gutermuth R. A., Hora J. L., Brunt, C. M., Muzerolle J. 2008, ApJ, 688, 1142 Onaka T. 2008, ApJL, 673, 147
- Kroupa P. 2001, MNRAS, 322, 231
- Kroupa P. 2002, Sci, 295, 82
- Landolt A.U. 1992, AJ, 104, 340
- Lang K.R. 1992, Astrophysical Data: Planets and Stars, (New York:Springer-Verlag), p. 132
- Lawson W.A., Fiegelson E.D., Huenemoerder D.P. 1996, MNRAS, 280, 1071
- Lefloch B., Lazareff B. 1994, A&A, 289, 559
- Lefloch B., Lazareff B. 1995, A&A, 301, 522
- Lefloch B., Lazareff B., Castets A. 1997, A&A, 324, 249
- Manoj P., Bhatt H.C., Maheswar G., Muneer S. 2006, ApJ, 653, 657
- Mart'in E.L. 1998, AJ, 115, 351
- Matsuyanagi I., Itoh Y., Sugitani K., Oasa Y., Mukai T., Tamura M. 2006, PASJ, 58, L29
- Megeath S. T., Allen L.E., Gutermuth R.A., et al. 2004, ApJS, 154, 367
- Meyer M., Calvet N., & Hillenbrand, L. A. 1997, AJ, 114, 288
- Miao J., White G.J., Nelson R., Thompson M., Morgan L. 2006, MNRAS, 369, 143
- Morgan L.K., Thompson M.A., Urquhart J.S., White G.J., Mio J. 2004, A&A, 426, 535
- Morgan L.K., Thompson M.A., Urquhart J.S., White G.J. 2008, A&A, 477, 557
- Muzerolle J., Calvet N., Hartmann, L. 2001, ApJ, 550, 994
- Nakano M., Sugitani K., Niwa T., Itoh Y., Watanabe M. 2008, PASJ, 60, 739
- Ogura K., Sugitani K., Pickles A. 2002, AJ, 123, 2597
- Ogura K., Chauhan N., Pandey A.K., Bhatt B.C., Ojha D.K., Itoh Y. 2007, PASJ, 59, 199 (Paper I)
- Ojha D.K., Tamura M., Nakajima Y., et al. 2004a, ApJ, 608, 797
- Ojha D.K., Tamura M., Nakajima Y., et al. 2004b, ApJ, 616, 1042
- Pandey A.K., Sharma S., Ogura K., Ojha D.K., Chen W.P., Bhatt B.C., Ghosh S.K. 2008, MNRAS, 383, 1241
- Patel N.A., Heyer M.H., Goldsmith P.F., Snell R.L., Hezel

- T., Pratap P. 1994, ASPC, 65, 81
- Patel N.A., Goldsmith P.F., Heyer M.H., Snell R.L., & Pratap P. 1998, ApJ, 507, 241
- Reach, W. et al., 2006, Infrared Array Camera Data Handbook, version 3.0, Spitzer Science Centre, California Institute of Technology, Pasadena, California 91125 USA
- Robitaille T.P., Whitney B.A., Indebetouw R., Wood K., Denzmore P. 2006, ApJS, 167, 256
- Samal M.R., Pandey A.K., Ojha D.K., Ghosh S.K., Kulkarni V.K., Bhatt B.C. 2007, ApJ, 671, 555
- Schaller G., Scherer D., Meynet G., & Maeder A. 1992, A&AS., 96, 269
- Sharma S., Pandey A.K., Ojha D.K., Chen W.P., Ghosh S.K., Bhatt B.C., Maheswar G., Sagar R. 2007, MNRAS, 380, 1141
- Shevchenko V. S, Ezhkova O. V., Ibrahimov, M. A., van den Ancker, M. E., Tjin A Djie H. R. E. 1999, MNRAS, 310, 210
- Siess L., Dufour E., Forestini M. 2000, A&A, 358, 593
- Sicilia-Aguilar A., Hartmann L.W., Briceno C., Muzerolle J., Calvet N. 2004, AJ, 128, 805
- Sicilia-Aguilar A., Hartmann L.W., Harnandez J., Briceno C., Calvet N. 2005, AJ, 130, 188
- Stetson P.B. 1987, PASP, 99, 191
- Sugitani K., Fukui Y., Ogura K. 1991, ApJS, 77, 59 (SFO91)
- Sugitani K., Ogura K. 1994, ApJS, 92, 163
- Sugitani K., Tamura M., Ogura K. 1995, ApJ, 455, L39
- Sung H., Chun M. Y., Bessel M.S. 2000, AJ, 120, 333
- Thompson M.A., White G.J., Morgan L.K., Miao J., Fridlund C.V.M., Huldtgren-White M., 2004, A&A, 414, 1017
- Vallee V. P., Hughes V.A., Viner M.R. 1979, A&A, 80, 189
- Walter F.M., Brown A. Matthieu R.D., Meyer P.C., Vrba F.J. 1988, AJ, 96, 297
- Whitney B.A., Wood K., Bjorkman J.E., & Cohen M. 2003, ApJ, 598, 1079
- Yang J., Fukui Y. 1992, ApJ, 386, 618

11 APPENDIX

APPENDIX A:

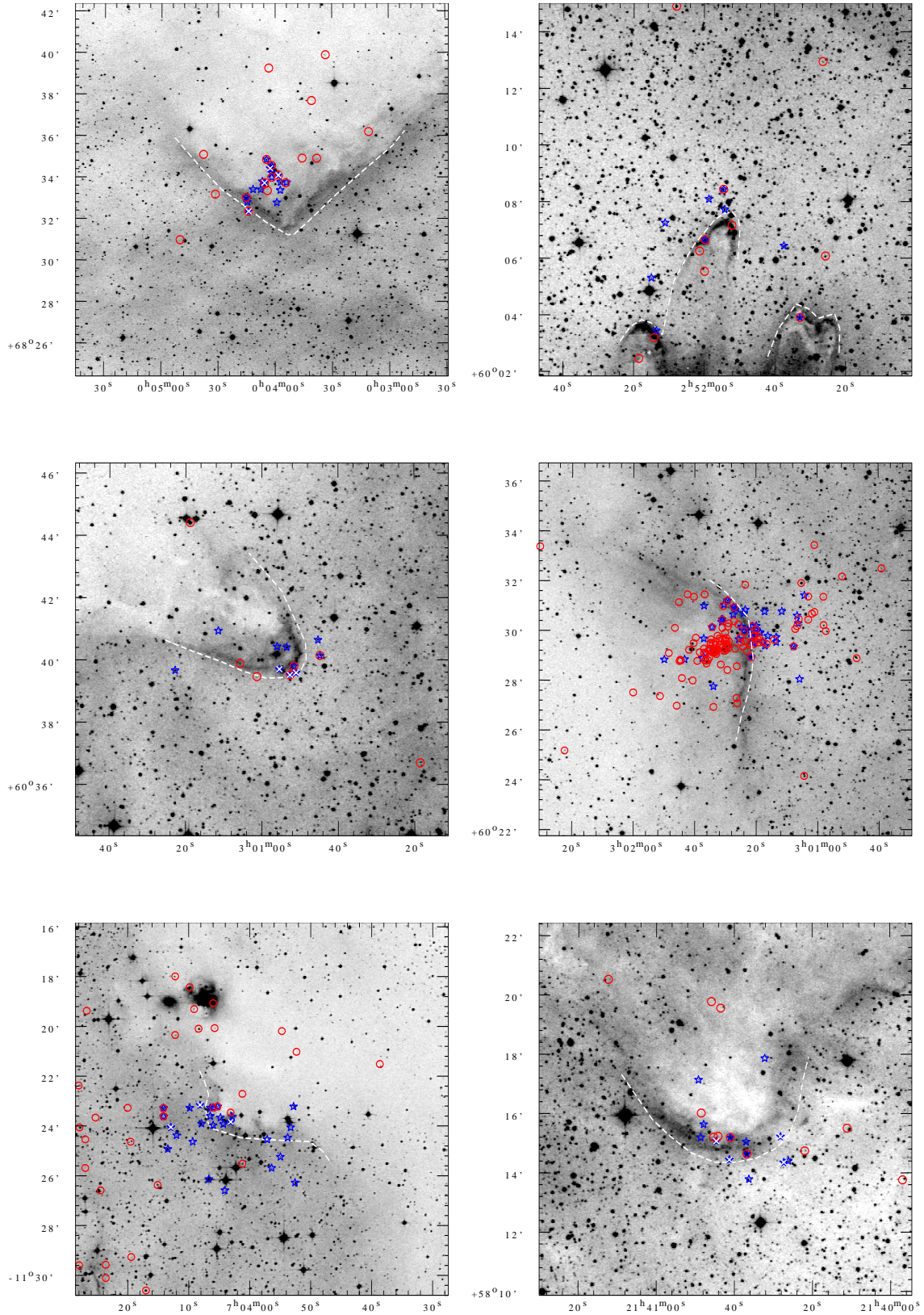


Figure A1. Spatial distribution of H α emission (star symbol) and NIR excess (open circle) stars overlaid on DSS2 R-band image of BRC 2 (upper – left panel); BRC 11NE (upper – right panel); BRC13 (middle – left panel); BRC 14 (middle – right panel); BRC27 (lower – left panel); BRC 38 (lower – right panel). Dashed line demarcates the regions on/ inside and outside bright-rims. White crosses represent H α emission stars having ages larger than 5 Myr (see sec. 7 and Fig. 9).

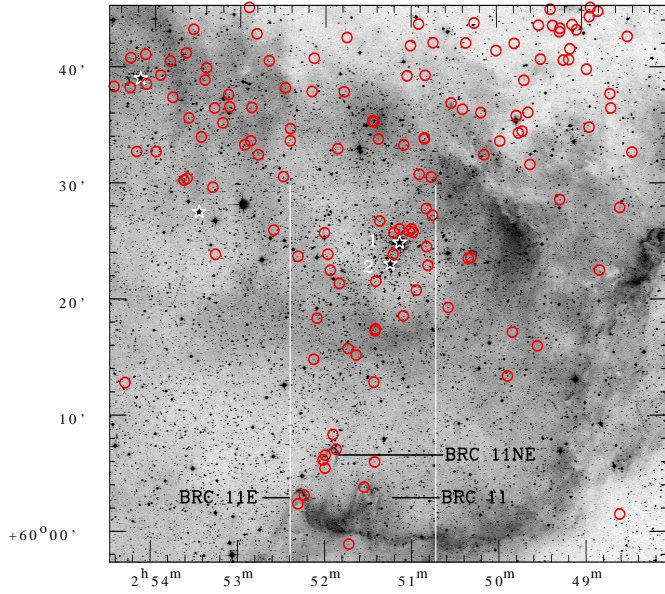


Figure A2. Spatial distribution of NIR excess stars (open circles) overlaid on DSS2 R-band image of the IC 1848W region. Star symbols indicate O type stars. The stars marked as ‘1’ and ‘2’ are HD 17505 (O6 V) and HD 17520 (O9 V) respectively. The variation of NIR excess $\Delta(H-K)$ and A_V for the stars within the strip as a function of distance from HD 17505 is shown in Fig. 6.

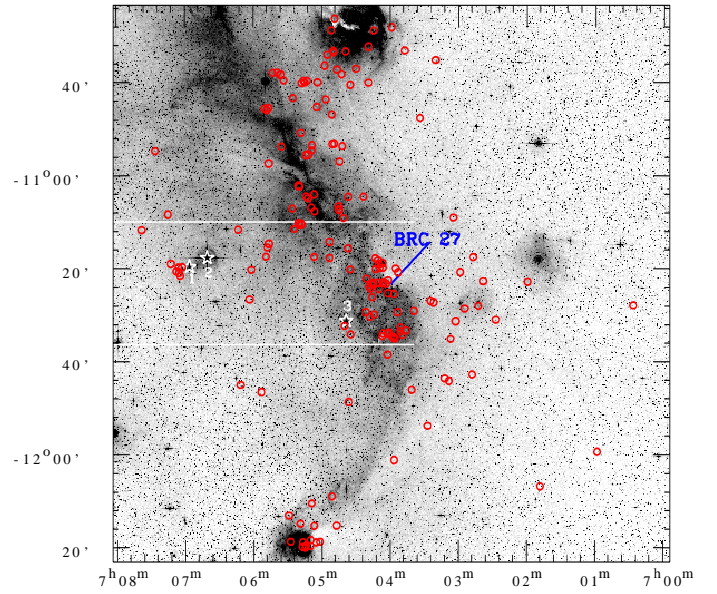


Figure A4. Same as Fig. A2 but for CMaR1 region. Stars marked as ‘1’, ‘2’ and ‘3’ are HD 54025 (B1 V); HD 53974 (B0.5 IV) and HD 53456 (B0 V) respectively.

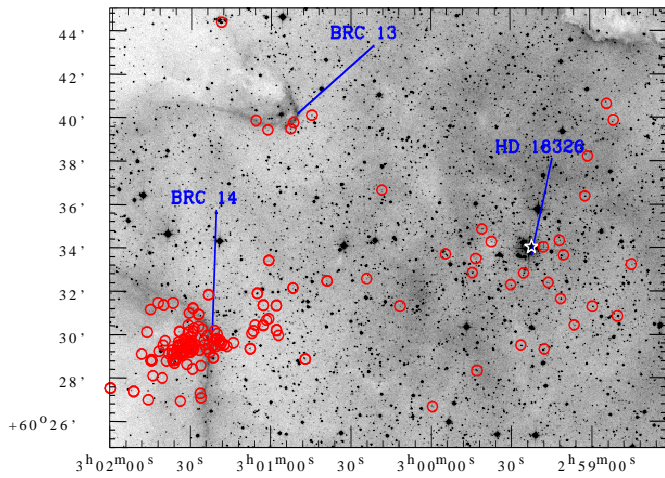


Figure A3. Same as Fig. A2 but for IC 1848E region.

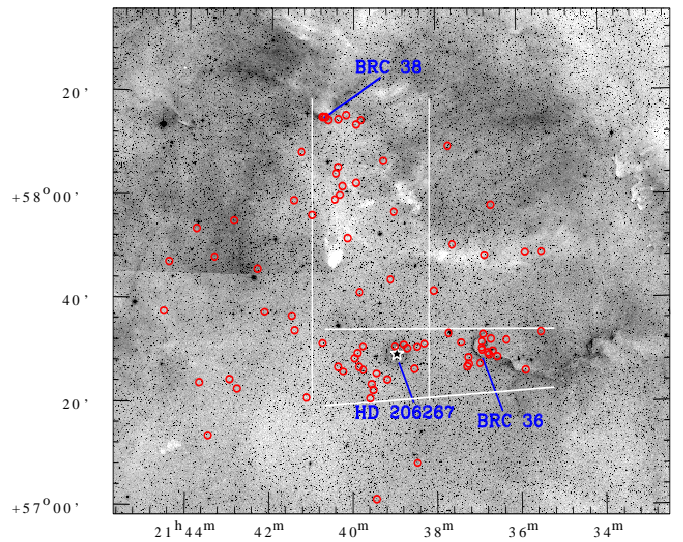


Figure A5. Same as Fig. A2 but for IC 1396.

Table 6. IRAC photometric magnitudes of the disk bearing candidates in BRCs 2, 27 and 13/14.

RA (J2000)	DEC (J2000)	[3.6]	e[3.6]	[4.5]	e[4.5]	[5.8]	e[4.5]	[8.0]	e[8.0]	IRAC type
BRC 2										
00 04 14.69	+68 32 49.8	11.899	0.033	10.97	0.03	10.095	0.052	8.985	0.028	0/I
00 03 57.27	+68 33 24.4	12.231	0.038	11.74	0.042	11.100	0.087	9.996	0.075	0/I
00 04 03.83	+68 32 49.6	13.316	0.064	12.57	0.062	11.749	0.123	10.57	0.117	0/I
00 03 59.71	+68 35 06.9	7.237	0.004	5.778	0.004	4.558	0.004	3.586	0.002	0/I
00 04 37.79	+68 35 07.4	10.274	0.015	9.342	0.014	8.595	0.027	7.630	0.026	0/I
00 03 57.78	+68 35 01.6	10.344	0.021	9.414	0.021	8.707	0.034	7.725	0.035	0/I
00 03 54.41	+68 35 17.8	11.283	0.024	9.973	0.019	8.938	0.031	8.048	0.021	0/I
00 04 03.90	+68 35 01.9	11.129	0.025	10.05	0.021	9.311	0.046	8.544	0.044	0/I
00 04 11.51	+68 36 01.0	11.481	0.027	10.38	0.023	9.602	0.042	8.748	0.032	0/I
00 03 56.17	+68 34 42.4	11.815	0.033	10.65	0.026	9.924	0.051	9.236	0.056	0/I
00 04 01.83	+68 34 35.2	7.925	0.006	7.318	0.006	6.815	0.012	5.996	0.008	II
00 04 15.21	+68 33 02.8	9.342	0.010	8.882	0.012	8.427	0.024	7.804	0.015	II
00 04 05.58	+68 33 45.0	9.231	0.010	8.604	0.011	8.129	0.021	7.318	0.016	II
00 03 33.24	+68 39 56.7	9.741	0.012	9.366	0.014	9.152	0.034	8.684	0.031	II
00 04 13.89	+68 32 22.5	10.119	0.014	9.532	0.015	9.101	0.033	8.461	0.020	II
00 03 57.05	+68 33 47.2	10.234	0.015	9.791	0.017	9.430	0.038	8.874	0.025	II
00 04 04.49	+68 34 53.2	10.477	0.017	9.997	0.020	9.546	0.043	8.830	0.036	II
00 04 12.17	+68 32 49.6	10.884	0.020	10.470	0.024	9.988	0.049	9.153	0.033	II
00 04 01.71	+68 34 01.1	10.897	0.020	10.460	0.024	10.002	0.050	9.258	0.034	II
00 03 58.26	+68 34 07.6	10.974	0.021	10.390	0.023	9.948	0.049	9.287	0.041	II
00 04 02.52	+68 34 27.5	10.970	0.025	10.480	0.028	10.033	0.056	9.097	0.035	II
00 04 35.38	+68 36 58.9	11.378	0.026	10.770	0.027	10.252	0.061	9.420	0.076	II
00 04 15.36	+68 34 06.4	11.532	0.028	11.050	0.031	10.626	0.069	9.861	0.060	II
00 04 11.63	+68 33 26.2	11.664	0.029	11.230	0.034	10.655	0.067	9.827	0.040	II
00 04 04.60	+68 33 49.8	11.089	0.031	10.330	0.028	9.702	0.049	8.777	0.049	II
00 03 55.64	+68 41 06.4	11.829	0.031	11.290	0.034	10.897	0.075	10.465	0.052	II
00 03 58.79	+68 34 49.7	11.640	0.033	11.090	0.037	10.521	0.105	9.940	0.097	II
00 03 54.42	+68 33 45.8	11.920	0.033	11.360	0.036	10.759	0.072	9.742	0.046	II
00 04 09.67	+68 32 33.1	11.988	0.034	11.910	0.046	11.782	0.113	11.287	0.084	II
00 04 07.31	+68 33 43.6	12.215	0.040	11.700	0.044	11.086	0.088	10.080	0.077	II
00 03 59.02	+68 32 48.4	12.370	0.041	11.910	0.046	11.353	0.103	10.612	0.150	II
00 03 53.69	+68 35 53.8	12.423	0.043	11.700	0.042	11.290	0.104	10.622	0.159	II
00 03 55.95	+68 33 35.1	12.629	0.046	12.270	0.054	11.846	0.124	10.906	0.093	II
00 03 54.86	+68 32 43.6	12.983	0.054	12.250	0.053	11.681	0.109	11.212	0.088	II
00 04 04.61	+68 34 44.1	12.85	0.057	12.280	0.073	11.672	0.121	11.089	0.165	II
BRC 27										
07 04 01.21	-11 22 43.2	8.412	0.007	7.614	0.007	6.874	0.012	5.166	0.005	0/I
07 04 12.56	-11 26 34.3	12.843	0.051	12.210	0.053	11.561	0.104	10.424	0.076	0/I
07 04 01.38	-11 23 35.5	9.419	0.011	9.076	0.013	8.627	0.035	7.839	0.051	II
07 04 03.14	-11 23 28.3	9.653	0.014	9.282	0.015	8.830	0.046	7.903	0.088	II
07 04 01.21	-11 25 31.9	10.587	0.018	10.201	0.021	9.964	0.049	9.368	0.032	II
07 04 02.89	-11 23 37.9	10.931	0.023	10.537	0.026	10.073	0.070	9.065	0.109	II
07 04 02.74	-11 23 25.9	11.135	0.026	10.657	0.027	10.038	0.078	9.050	0.124	II
07 04 05.21	-11 23 13.9	11.371	0.026	10.914	0.029	10.384	0.062	9.415	0.051	II
07 04 05.95	-11 23 59.5	11.620	0.029	11.097	0.031	10.621	0.066	9.691	0.050	II
07 04 04.71	-11 23 40.3	11.631	0.030	11.238	0.034	10.971	0.101	10.239	0.184	II
07 04 08.04	-11 23 55.3	11.908	0.033	11.773	0.043	11.680	0.109	11.225	0.091	II
07 04 01.62	-11 21 33.0	11.968	0.034	11.623	0.040	11.174	0.092	10.545	0.113	II
07 04 06.57	-11 23 16.7	12.08	0.039	11.802	0.045	11.231	0.111	10.179	0.132	II
07 04 03.09	-11 23 51.1	12.021	0.041	11.720	0.044	10.559	0.094	9.671	0.210	II
07 04 02.14	-11 25 12.7	12.504	0.043	12.071	0.049	11.864	0.117	11.145	0.077	II
07 04 06.44	-11 23 36.7	12.635	0.047	12.405	0.058	12.049	0.131	11.631	0.160	II
07 04 06.03	-11 23 16.3	12.668	0.048	12.096	0.05	11.508	0.109	10.499	0.109	II
07 04 01.28	-11 22 34.2	12.969	0.055	12.65	0.066	12.247	0.149	11.421	0.167	II
BRC 14										
03 01 21.66	+60 28 55.6	8.563	0.007	8.080	0.008	7.378	0.015	6.259	0.008	0/I
03 02 21.76	+60 25 57.3	10.643	0.018	10.164	0.020	9.562	0.041	8.163	0.018	0/I
03 00 27.55	+60 27 35.2	10.864	0.020	10.452	0.023	9.873	0.047	8.579	0.021	0/I
03 01 34.55	+60 28 48.9	11.154	0.031	10.538	0.030	9.907	0.110	8.713	0.111	0/I
03 00 52.78	+60 40 15.4	12.264	0.041	11.665	0.042	10.807	0.090	9.551	0.082	0/I
03 00 56.49	+60 40 11.0	10.087	0.047	9.568	0.034	7.799	0.095	6.098	0.095	0/I
03 00 56.85	+60 40 29.0	11.307	0.053	10.625	0.043	9.929	0.076	8.622	0.075	0/I

Table 6 cont.

03 01 32.14	+60 26 48.9	13.510	0.073	13.064	0.079	12.478	0.215	11.100	0.234	0/I
03 00 55.39	+60 45 21.8	13.864	0.081	13.322	0.088	11.816	0.115	9.827	0.042	0/I
03 01 48.00	+60 35 22.9	13.194	0.088	12.325	0.059	11.115	0.131	9.658	0.144	0/I
03 00 53.09	+60 40 36.5	13.176	0.093	12.375	0.065	11.151	0.139	9.229	0.095	0/I
03 01 32.47	+60 25 53.7	10.677	0.019	9.344	0.015	8.289	0.023	7.266	0.013	0/I
03 01 48.54	+60 29 05.1	10.980	0.021	10.109	0.020	9.219	0.035	8.442	0.021	0/I
03 01 43.43	+60 28 50.2	11.130	0.025	10.327	0.025	9.835	0.046	9.098	0.041	0/I
03 01 32.10	+60 29 40.5	11.271	0.035	10.262	0.030	9.418	0.067	8.620	0.071	0/I
03 01 36.08	+60 28 37.4	11.875	0.038	10.768	0.030	9.922	0.052	9.341	0.044	0/I
03 01 52.90	+60 24 48.3	12.354	0.040	11.231	0.033	10.245	0.056	9.333	0.032	0/I
03 01 39.41	+60 29 27.7	12.352	0.043	11.224	0.034	10.374	0.062	9.634	0.061	0/I
03 01 20.86	+60 31 23.5	14.230	0.094	13.261	0.085	12.674	0.172	11.694	0.091	0/I
03 01 20.31	+60 29 48.3	9.109	0.009	8.615	0.010	8.209	0.022	7.503	0.013	II
03 01 30.15	+60 29 54.6	10.099	0.015	9.497	0.016	9.186	0.036	8.637	0.050	II
03 01 05.24	+60 31 54.4	10.126	0.015	9.756	0.017	9.410	0.038	8.514	0.021	II
03 01 41.20	+60 29 15.3	10.556	0.018	10.491	0.024	10.462	0.071	9.611	0.057	II
03 01 44.92	+60 28 48.9	10.611	0.019	9.993	0.020	9.451	0.040	8.867	0.032	II
03 00 51.08	+60 39 34.9	10.811	0.020	10.328	0.022	10.030	0.050	9.344	0.032	II
03 01 29.32	+60 31 12.8	10.956	0.021	10.433	0.023	9.969	0.049	9.279	0.036	II
03 01 07.75	+60 29 20.9	11.087	0.022	10.665	0.026	10.35	0.058	9.794	0.038	II
03 00 25.58	+60 28 08.7	11.302	0.024	10.984	0.030	10.709	0.069	9.691	0.035	II
03 01 34.37	+60 30 07.7	11.230	0.025	10.751	0.027	10.167	0.065	9.246	0.078	II
03 01 16.63	+60 30 53.5	11.402	0.026	11.128	0.032	10.885	0.075	10.343	0.048	II
03 02 22.56	+60 25 09.3	11.490	0.027	11.053	0.031	10.682	0.068	9.617	0.040	II
03 00 44.78	+60 40 08.3	11.624	0.028	11.084	0.031	10.611	0.066	9.880	0.039	II
03 01 04.37	+60 24 08.7	11.654	0.029	11.260	0.034	10.912	0.075	10.249	0.046	II
03 01 38.96	+60 25 31.0	11.677	0.029	11.647	0.040	11.448	0.105	10.814	0.129	II
03 01 25.80	+60 29 18.1	11.367	0.030	10.922	0.034	9.894	0.113	8.917	0.088	II
03 00 54.43	+60 39 38.1	11.734	0.031	11.521	0.039	11.066	0.099	10.057	0.109	II
03 01 30.22	+60 29 36.9	10.655	0.031	9.955	0.031	9.611	0.08	9.081	0.108	II
03 00 57.25	+60 32 42.2	11.845	0.032	11.451	0.037	11.139	0.084	10.640	0.056	II
03 00 56.28	+60 32 34.4	11.842	0.032	11.614	0.04	11.401	0.095	10.896	0.063	II
03 01 54.81	+60 24 21.4	11.925	0.033	11.493	0.038	11.002	0.079	10.354	0.050	II
03 01 26.40	+60 30 52.9	11.901	0.033	11.667	0.041	11.267	0.093	10.525	0.089	II
03 01 20.27	+60 30 01.4	11.961	0.034	11.361	0.036	10.940	0.078	10.238	0.052	II
03 01 03.09	+60 41 30.4	11.963	0.034	11.874	0.045	11.557	0.124	10.856	0.204	II
03 00 57.98	+60 30 12.2	12.158	0.036	11.729	0.042	11.389	0.094	10.736	0.061	II
03 01 01.27	+60 28 38.6	12.192	0.037	11.853	0.045	11.415	0.095	10.660	0.056	II
03 00 56.85	+60 29 57.8	12.246	0.038	11.962	0.047	11.655	0.108	11.194	0.094	II
03 00 24.06	+60 26 15.7	12.262	0.038	12.258	0.054	11.958	0.123	11.342	0.077	II
03 01 18.78	+60 29 55.6	12.275	0.039	11.778	0.044	11.301	0.092	10.693	0.065	II
03 00 46.48	+60 39 51.5	12.421	0.041	11.914	0.046	11.548	0.101	10.759	0.059	II
03 00 45.33	+60 40 38.3	12.427	0.041	12.064	0.049	11.665	0.107	10.825	0.061	II
03 00 47.14	+60 28 52.7	12.407	0.041	12.084	0.049	11.777	0.112	11.131	0.070	II
03 01 22.84	+60 39 39.2	12.425	0.041	12.086	0.049	11.831	0.116	10.850	0.061	II
03 01 22.45	+60 30 02.0	12.337	0.040	11.968	0.048	11.590	0.109	10.903	0.098	II
03 00 45.26	+60 31 16.7	12.485	0.042	12.123	0.050	11.725	0.110	11.073	0.068	II
03 00 48.19	+60 31 08.4	12.455	0.042	12.226	0.053	11.991	0.125	11.323	0.078	II
03 01 21.21	+60 30 09.2	12.544	0.044	12.021	0.049	11.780	0.116	11.147	0.087	II
03 01 35.05	+60 27 56.0	12.478	0.044	12.372	0.057	12.515	0.193	11.722	0.209	II
03 00 48.68	+60 39 33.6	12.589	0.044	12.408	0.058	12.075	0.132	11.672	0.096	II
03 01 59.87	+60 24 18.2	12.592	0.044	12.539	0.061	12.373	0.154	11.905	0.181	II
03 00 41.93	+60 39 48.6	12.628	0.046	12.184	0.053	11.708	0.109	10.835	0.061	II
03 01 04.22	+60 31 24.4	12.673	0.046	12.200	0.052	11.943	0.122	11.259	0.074	II
03 01 31.72	+60 34 02.1	12.686	0.046	12.361	0.056	11.930	0.121	11.246	0.073	II
03 00 48.23	+60 39 33.0	12.635	0.046	12.395	0.057	12.047	0.130	11.541	0.091	II
03 01 54.04	+60 32 48.1	12.720	0.047	12.369	0.057	11.994	0.127	11.324	0.099	II
03 01 47.49	+60 28 10.6	12.754	0.048	12.289	0.054	11.874	0.120	11.129	0.088	II
03 00 42.59	+60 24 36.5	12.776	0.048	12.418	0.058	12.159	0.134	11.338	0.075	II
03 00 22.65	+60 31 42.1	12.691	0.048	12.486	0.060	12.194	0.140	11.616	0.089	II
03 01 40.78	+60 43 37.5	12.775	0.048	12.691	0.065	12.465	0.161	11.859	0.136	II
03 00 54.35	+60 36 49.9	12.745	0.048	12.721	0.066	12.719	0.176	12.140	0.186	II
03 00 57.31	+60 30 35.3	12.822	0.049	12.470	0.059	12.204	0.137	11.516	0.084	II
03 00 42.25	+60 29 12.7	12.895	0.051	12.419	0.058	12.201	0.138	11.623	0.097	II
03 01 12.99	+60 28 50.9	12.913	0.051	12.493	0.060	12.128	0.132	11.424	0.081	II
03 00 24.85	+60 33 13.5	12.888	0.051	12.653	0.065	12.492	0.159	11.800	0.108	II
03 01 35.79	+60 22 23.6	12.856	0.050	12.303	0.055	11.761	0.112	11.092	0.079	II
03 01 17.64	+60 24 24.3	12.857	0.050	12.502	0.060	11.948	0.124	10.977	0.070	II

Table 6 cont.

03 02 26.07	+60 33 02.8	12.837	0.050	12.819	0.070	12.613	0.179	11.726	0.192	II
03 01 31.04	+60 30 26.1	12.750	0.052	12.322	0.056	11.634	0.129	10.575	0.154	II
03 01 06.26	+60 30 16.8	12.962	0.052	12.536	0.061	12.177	0.135	11.566	0.084	II
03 01 49.97	+60 28 49.3	12.902	0.053	12.367	0.057	11.797	0.117	10.758	0.092	II
03 01 07.27	+60 25 25.7	13.011	0.054	12.520	0.061	11.887	0.119	11.122	0.076	II
03 01 08.16	+60 39 00.5	13.070	0.055	12.627	0.063	12.271	0.142	11.639	0.106	II
03 02 28.02	+60 32 21.2	13.074	0.055	13.035	0.077	12.920	0.200	12.362	0.193	II
03 00 46.58	+60 31 58.4	13.122	0.056	12.615	0.063	12.410	0.152	11.718	0.095	II
03 01 12.21	+60 38 40.2	13.118	0.057	12.458	0.059	12.034	0.127	11.468	0.090	II
03 00 52.69	+60 39 21.7	13.093	0.057	13.069	0.079	13.028	0.219	12.568	0.201	II
03 00 27.63	+60 28 46.3	13.159	0.058	12.968	0.074	12.938	0.196	12.236	0.125	II
03 00 53.24	+60 32 01.3	13.295	0.061	13.027	0.076	12.743	0.177	12.202	0.116	II
03 01 10.59	+60 25 55.8	13.253	0.060	12.701	0.066	12.203	0.138	11.753	0.094	II
03 00 36.20	+60 34 17.7	13.281	0.062	13.048	0.078	12.721	0.176	12.050	0.111	II
03 01 16.15	+60 29 46.3	13.327	0.063	13.002	0.076	12.769	0.182	12.173	0.124	II
03 01 10.75	+60 32 45.0	13.357	0.063	13.057	0.078	12.844	0.186	12.273	0.135	II
03 00 24.14	+60 32 35.1	13.337	0.064	12.869	0.071	12.302	0.145	11.383	0.080	II
03 02 01.70	+60 39 27.4	13.352	0.064	12.996	0.076	12.588	0.174	11.634	0.127	II
03 00 43.96	+60 34 50.2	13.415	0.065	12.964	0.074	12.828	0.184	12.178	0.124	II
03 01 22.23	+60 39 28.3	13.438	0.066	13.287	0.087	12.963	0.198	12.400	0.134	II
03 01 59.06	+60 22 57.4	13.494	0.067	13.342	0.089	13.208	0.230	12.579	0.243	II
03 00 44.00	+60 30 58.2	13.506	0.068	13.347	0.089	13.317	0.240	12.822	0.185	II
03 01 02.67	+60 31 00.9	13.533	0.069	13.506	0.096	13.396	0.247	12.776	0.184	II
03 00 30.81	+60 31 01.7	13.597	0.071	13.088	0.079	12.701	0.174	11.902	0.102	II
03 00 23.45	+60 31 50.6	13.527	0.071	13.111	0.081	13.042	0.213	12.438	0.138	II
03 01 40.12	+60 22 17.3	13.540	0.070	13.116	0.080	12.590	0.179	11.619	0.162	II
03 01 04.04	+60 28 23.2	13.588	0.070	13.243	0.084	12.989	0.199	12.446	0.154	II
03 00 46.60	+60 23 26.4	13.587	0.070	13.301	0.087	12.973	0.197	12.343	0.127	II
03 00 22.81	+60 28 26.6	13.678	0.074	13.482	0.095	13.309	0.242	12.805	0.166	II
03 01 17.14	+60 30 45.1	13.737	0.076	13.348	0.089	13.386	0.244	12.783	0.156	II
03 00 36.16	+60 24 12.2	13.757	0.076	13.658	0.103	13.438	0.247	12.947	0.180	II
03 00 50.07	+60 30 55.0	13.775	0.077	13.412	0.092	12.966	0.198	12.118	0.112	II
03 01 18.46	+60 29 47.5	13.365	0.079	12.91	0.085	12.421	0.162	11.869	0.136	II
03 00 46.71	+60 31 40.2	13.792	0.079	13.086	0.079	12.662	0.174	11.973	0.111	II
03 00 34.68	+60 27 43.9	13.831	0.079	13.481	0.094	13.326	0.235	12.827	0.156	II
03 00 45.01	+60 35 19.8	13.867	0.081	13.299	0.088	12.680	0.176	11.814	0.135	II
03 01 16.15	+60 31 30.7	13.888	0.080	13.321	0.087	12.959	0.196	12.319	0.122	II
03 00 27.18	+60 35 44.2	13.935	0.082	13.618	0.101	13.137	0.214	12.640	0.157	II
03 01 53.77	+60 29 21.4	13.892	0.082	13.729	0.107	13.303	0.241	12.219	0.194	II
03 01 05.84	+60 28 02.0	13.955	0.085	13.506	0.096	12.987	0.202	12.232	0.118	II
03 00 43.01	+60 31 08.3	14.013	0.086	13.612	0.100	13.058	0.207	12.098	0.114	II
03 01 31.55	+60 34 11.7	13.899	0.087	13.458	0.094	13.157	0.215	12.666	0.150	II
03 00 57.52	+60 29 18.2	14.044	0.087	13.477	0.094	12.851	0.186	11.931	0.108	II
03 01 45.15	+60 40 02.2	14.032	0.087	13.628	0.101	13.377	0.250	12.461	0.216	II
03 01 06.66	+60 30 35.3	14.045	0.087	13.632	0.101	13.337	0.234	12.618	0.159	II
03 01 25.74	+60 31 17.1	14.117	0.090	13.763	0.107	13.348	0.243	12.920	0.242	II
03 01 05.23	+60 29 20.6	14.169	0.092	13.589	0.099	13.196	0.225	12.689	0.160	II
03 00 42.87	+60 34 22.6	14.228	0.094	13.677	0.103	13.335	0.234	12.900	0.182	II
03 00 30.47	+60 31 16.5	14.244	0.096	13.830	0.111	13.297	0.230	12.456	0.136	II
03 00 39.02	+60 37 09.6	14.387	0.101	13.988	0.119	13.457	0.248	12.831	0.182	II

Table 7. *J*, *H* and *K* magnitudes of the sources used in the analysis (cf. sec. 6.2)

RA (J2000)	DEC (J2000)	2MASS Name	<i>J</i> ± e <i>J</i> (mag)	<i>H</i> ± e <i>H</i> (mag)	<i>K</i> ± e <i>K</i> (mag)	Q flag	C flag	<i>A_V</i> (mag)	Δ(<i>H</i> − <i>K</i>) (mag)	2MASS/Matsuyana et al. 2006(M06)
IC 1848W										
02 51 12.63	+60 24 00.1	02511262+6024000	13.719 ± 0.050	12.912 ± 0.051	12.361 ± 0.035	AAA	000	0.00	0.05	2MASS
02 51 24.86	+60 21 40.2	02512485+6021402	14.305 ± 0.038	13.545 ± 0.043	13.017 ± 0.031	AAA	000	0.00	0.05	2MASS
02 51 12.27	+60 25 51.3	02511226+6025512	15.955 ± 0.086	15.189 ± 0.103	14.630 ± 0.099	AAA	c00	0.00	0.08	2MASS
02 51 08.31	+60 26 09.9	02510831+6026099	14.390 ± 0.075	13.636 ± 0.065	13.160 ± 0.062	AAA	000	0.00	0.01	2MASS
02 50 56.55	+60 20 53.1	02505654+6020530	15.257 ± 0.060	14.296 ± 0.066	13.646 ± 0.043	AAA	ccc	0.69	0.07	2MASS
02 50 48.48	+60 23 02.1	02504848+6023020	16.032 ± 0.072	15.269 ± 0.084	14.691 ± 0.095	AAA	000	0.00	0.10	2MASS
02 51 01.47	+60 25 58.9	02510147+6025589	15.908 ± 0.087	15.131 ± 0.088	14.618 ± 0.092	AAA	c00	0.00	0.03	2MASS
02 50 58.77	+60 25 53.7	02505876+6025536	15.497 ± 0.074	14.396 ± 0.065	13.687 ± 0.067	AAA	ccc	2.00	0.05	2MASS
02 50 49.41	+60 24 38.4	02504941+6024384	14.625 ± 0.055	13.629 ± 0.042	12.767 ± 0.026	AAA	000	0.00	0.26	2MASS
02 50 59.84	+60 26 10.6	02505983+6026105	15.258 ± 0.080	14.224 ± 0.074	13.555 ± 0.051	AAA	000	1.47	0.05	2MASS
02 51 22.13	+60 26 51.2	02512213+6026512	14.030 ± 0.042	12.804 ± 0.030	12.007 ± 0.021	AAA	000	2.89	0.07	2MASS
02 51 49.74	+60 21 28.5	02514973+6021285	14.941 ± 0.032	14.059 ± 0.040	13.455 ± 0.034	AAA	ccc	0.06	0.06	2MASS
02 51 05.64	+60 18 40.7	02510563+6018406	15.072 ± 0.025	13.820 ± 0.041	12.967 ± 0.030	AAA	000	2.77	0.11	2MASS
02 51 56.56	+60 22 35.8	02515655+6022358	15.669 ± 0.070	14.766 ± 0.079	14.208 ± 0.066	AAA	ccc	0.69	0.01	2MASS
02 51 58.31	+60 23 59.2	02515831+6023591	15.386 ± 0.045	14.358 ± 0.045	13.569 ± 0.047	AAA	000	0.43	0.17	2MASS
02 51 25.03	+60 17 32.9	02512502+6017329	14.732 ± 0.035	13.639 ± 0.036	12.967 ± 0.027	AAA	000	2.20	0.02	2MASS
02 50 45.22	+60 27 21.6	02504522+6027216	15.651 ± 0.088	14.433 ± 0.072	13.507 ± 0.062	AAA	cc0	1.75	0.20	2MASS
02 51 25.44	+60 17 23.2	02512544+6017231	15.603 ± 0.070	14.313 ± 0.038	13.281 ± 0.034	AAA	000	1.81	0.27	2MASS
02 50 49.61	+60 27 55.3	02504960+6027553	15.067 ± 0.048	13.981 ± 0.068	13.295 ± 0.057	AAA	ccc	1.99	0.03	2MASS
02 52 00.71	+60 25 49.8	02520071+6025497	15.998 ± 0.081	15.223 ± 0.098	14.700 ± 0.098	AAA	c00	0.66	0.04	2MASS
02 52 05.71	+60 18 28.1	02520571+6018281	15.513 ± 0.070	14.744 ± 0.066	14.233 ± 0.076	AAA	cc0	0.00	0.03	2MASS
02 52 19.20	+60 23 48.1	02521920+6023481	15.478 ± 0.072	14.562 ± 0.079	13.835 ± 0.058	AAA	000	0.00	0.17	2MASS
02 51 44.25	+60 15 51.7	02514424+6015517	15.911 ± 0.092	15.040 ± 0.093	14.489 ± 0.092	AAA	000	0.34	0.02	2MASS
02 51 38.48	+60 15 18.1	02513847+6015181	16.121 ± 0.091	15.214 ± 0.083	14.564 ± 0.088	AAA	000	0.01	0.10	2MASS
02 51 26.18	+60 12 57.7	02512618+6012576	15.985 ± 0.071	15.208 ± 0.099	14.662 ± 0.088	AAA	000	0.00	0.06	2MASS
02 52 07.87	+60 14 55.6	02520787+6014556	14.372 ± 0.026	13.354 ± 0.036	12.574 ± 0.028	AAA	000	0.00	0.16	2MASS
02 51 54.52	+60 08 26.6	02515451+6008266	14.582 ± 0.056	13.567 ± 0.043	12.825 ± 0.038	AAA	c0c	0.64	0.13	2MASS
02 51 52.12	+60 07 10.2	02515212+6007102	14.131 ± 0.032	12.975 ± 0.033	12.136 ± 0.026	AAA	000	1.66	0.15	2MASS
02 51 25.58	+60 06 04.8	02512557+6006048	14.609 ± 0.038	13.142 ± 0.033	12.095 ± 0.019	AAA	000	3.95	0.19	2MASS
02 51 59.76	+60 06 39.5	02515975+6006394	15.306 ± 0.048	14.236 ± 0.042	13.515 ± 0.038	AAA	000	1.51	0.08	2MASS
02 52 01.32	+60 06 15.4	02520131+6006154	15.629 ± 0.053	14.406 ± 0.056	13.627 ± 0.042	AAA	000	2.99	0.05	2MASS
02 51 59.93	+60 05 32.3	02515993+6005323	16.155 ± 0.091	14.914 ± 0.081	14.142 ± 0.068	AAA	000	3.28	0.04	2MASS
02 51 32.84	+60 03 54.2	02513283+6003542	13.005 ± 0.026	11.523 ± 0.032	10.447 ± 0.022	AAA	000	3.90	0.21	2MASS
02 52 14.22	+60 03 11.4	02521422+6003114	14.311 ± 0.036	13.278 ± 0.038	12.532 ± 0.032	AAA	000	0.84	0.12	2MASS
02 52 18.56	+60 02 27.4	02521856+6002274	16.212 ± 0.107	15.204 ± 0.095	14.272 ± 0.069	AAA	000	0.00	0.32	2MASS
02 51 43.36	+59 58 59.7	02514336+5958597	16.005 ± 0.089	15.139 ± 0.096	14.583 ± 0.092	AAA	000	0.24	0.02	2MASS
IC 1848E										
03 01 33.0	+60 29 04		17.25 ± 0.02	15.85 ± 0.02	14.82 ± 0.02			3.91	0.20	M06
03 01 33.9	+60 29 09		14.35 ± 0.01	13.25 ± 0.01	12.54 ± 0.01			2.33	0.06	M06
03 01 36.4	+60 29 06		15.66 ± 0.01	14.18 ± 0.01	13.12 ± 0.01			4.78	0.18	M06
03 01 33.2	+60 29 08		17.37 ± 0.07	15.64 ± 0.04	14.37 ± 0.03			6.55	0.25	M06
03 01 34.3	+60 29 08		16.16 ± 0.03	15.07 ± 0.03	14.13 ± 0.03			6.34	0.29	M06
03 01 34.0	+60 29 10		14.81 ± 0.01	13.69 ± 0.01	12.95 ± 0.01			2.36	0.08	M06
03 01 35.4	+60 29 11		16.76 ± 0.04	14.88 ± 0.03	13.49 ± 0.02			7.66	0.28	M06
03 01 30.1	+60 29 12		14.52 ± 0.01	13.41 ± 0.02	12.61 ± 0.02			1.74	0.14	M06
03 01 33.0	+60 29 12		16.97 ± 0.04	15.65 ± 0.04	14.59 ± 0.05			2.56	0.28	M06
03 01 33.4	+60 29 13		16.60 ± 0.02	15.49 ± 0.02	14.70 ± 0.04			1.82	0.13	M06
03 01 35.4	+60 29 15		17.62 ± 0.09	16.22 ± 0.04	15.05 ± 0.01			2.79	0.34	M06
03 01 32.7	+60 29 16		17.53 ± 0.08	15.17 ± 0.03	13.54 ± 0.02			12.37	0.23	M06
03 01 34.9	+60 29 16		15.10 ± 0.01	13.23 ± 0.01	11.68 ± 0.01			6.24	0.44	M06
03 01 29.8	+60 29 19		16.80 ± 0.04	15.61 ± 0.05	14.70 ± 0.05			1.97	0.20	M06
03 01 29.1	+60 29 18		17.63 ± 0.06	16.60 ± 0.07	15.72 ± 0.08			0.00	0.27	M06
03 01 30.9	+60 29 19		14.30 ± 0.01	12.89 ± 0.01	11.86 ± 0.01			4.05	0.20	M06
03 01 26.8	+60 29 17		18.80 ± 0.09	16.31 ± 0.01	14.56 ± 0.01			13.21	0.28	M06
03 01 33.2	+60 29 26		17.15 ± 0.03	15.63 ± 0.02	14.53 ± 0.01			5.01	0.20	M06
03 01 31.9	+60 29 26		15.27 ± 0.01	12.87 ± 0.01	11.26 ± 0.01			13.09	0.19	M06
03 01 29.6	+60 29 28		17.69 ± 0.03	16.39 ± 0.02	15.46 ± 0.04			3.33	0.16	M06
03 01 34.8	+60 29 31		16.85 ± 0.01	15.72 ± 0.01	14.87 ± 0.01			1.62	0.18	M06
03 01 29.6	+60 29 35		17.28 ± 0.03	15.97 ± 0.04	15.05 ± 0.05			3.55	0.14	M06
03 01 23.3	+60 29 34		18.35 ± 0.04	16.66 ± 0.02	15.28 ± 0.01			5.11	0.38	M06
03 01 32.0	+60 29 36		17.60 ± 0.02	16.55 ± 0.03	15.72 ± 0.03			0.67	0.21	M06
03 01 30.2	+60 29 37		16.95 ± 0.02	14.55 ± 0.01	12.88 ± 0.01			12.61	0.25	M06
03 01 34.7	+60 29 39		18.62 ± 0.04	17.62 ± 0.03	16.86 ± 0.04			0.54	0.17	M06
03 01 30.2	+60 29 39		16.86 ± 0.02	14.45 ± 0.01	12.86 ± 0.01			13.39	0.16	M06
03 01 30.9	+60 29 40		19.33 ± 0.10	17.76 ± 0.06	16.64 ± 0.07			5.54	0.19	M06
03 01 32.0	+60 29 41		18.70 ± 0.05	16.12 ± 0.02	14.33 ± 0.01			14.13	0.26	M06
03 01 29.8	+60 29 43		18.23 ± 0.03	16.59 ± 0.02	15.41 ± 0.01			6.03	0.21	M06
03 01 25.1	+60 29 44		17.31 ± 0.01	15.42 ± 0.01	14.14 ± 0.01			8.68	0.16	M06
03 01 32.6	+60 29 48		18.20 ± 0.03	15.87 ± 0.01	14.14 ± 0.01			11.16	0.35	M06
03 01 30.1	+60 29 55	03013009+6029554	14.64 ± 0.01	12.86 ± 0.01	11.69 ± 0.01			8.04	0.12	M06
03 01 23.8	+60 29 59	0301238+6029587	16.15 ± 0.01	14.95 ± 0.01	14.16 ± 0.01			3.07	0.08	M06

Table 7 cont.

03 01 31.0	+60 30 07		19.27 ± 0.06	17.81 ± 0.04	16.79 ± 0.03		4.82	0.16	M06
03 01 29.2	+60 30 10		16.35 ± <0.01	14.64 ± <0.01	13.54 ± <0.01		7.64	0.09	M06
03 01 28.9	+60 30 18		19.09 ± 0.05	18.04 ± 0.04	17.27 ± 0.04		1.15	0.15	M06
03 01 31.0	+60 30 27		16.33 ± 0.01	15.10 ± 0.01	14.29 ± <0.01		3.32	0.08	M06
03 01 30.7	+60 30 60		17.96 ± 0.02	16.54 ± 0.01	15.60 ± 0.01		4.91	0.10	M06
03 01 29.3	+60 31 13		14.72 ± <0.01	13.42 ± <0.01	12.42 ± <0.01		2.77	0.23	M06
03 01 45.9	+60 26 59		19.64 ± 0.10	18.46 ± 0.08	17.54 ± 0.07		1.75	0.22	M06
03 01 40.7	+60 28 00		18.80 ± 0.05	17.51 ± 0.04	16.58 ± 0.04		3.19	0.17	M06
03 01 45.0	+60 28 47		16.76 ± 0.01	15.24 ± 0.01	14.13 ± 0.01		4.93	0.21	M06
03 01 39.2	+60 28 47		17.81 ± 0.02	16.44 ± 0.01	15.54 ± 0.01		4.54	0.09	M06
03 01 44.5	+60 28 48		17.97 ± 0.03	16.45 ± 0.02	15.34 ± 0.02		4.93	0.21	M06
03 01 36.7	+60 28 48		16.72 ± 0.02	15.57 ± 0.01	14.82 ± 0.01		2.70	0.07	M06
03 01 44.8	+60 28 50	03014484+6028496	15.96 ± 0.01	13.98 ± 0.01	12.55 ± <0.01		8.72	0.26	M06
03 01 48.5	+60 29 06		17.38 ± 0.02	15.83 ± 0.01	14.30 ± 0.01		1.97	0.61	M06
03 01 37.0	+60 29 07		16.51 ± 0.01	14.95 ± 0.01	13.86 ± <0.01		5.64	0.17	M06
03 01 38.4	+60 29 08		18.67 ± 0.05	17.28 ± 0.04	16.13 ± 0.03		2.81	0.33	M06
03 01 41.9	+60 29 14		17.73 ± 0.03	15.97 ± 0.01	14.77 ± 0.01		7.52	0.16	M06
03 01 37.0	+60 29 17		18.66 ± 0.05	16.12 ± 0.01	14.44 ± 0.01	14.46	0.18	M06	
03 01 40.4	+60 29 30		18.04 ± 0.03	16.43 ± 0.02	15.15 ± 0.01		4.81	0.33	M06
03 01 39.7	+60 29 43		17.36 ± 0.02	15.47 ± 0.01	14.24 ± <0.01		9.08	0.11	M06
03 01 46.5	+60 30 07		19.27 ± 0.07	18.23 ± 0.06	17.40 ± 0.06		0.53	0.21	M06
03 01 27.2	+60 30 23		19.49 ± 0.09	17.69 ± 0.04	16.44 ± 0.03		7.68	0.18	M06
03 01 45.2	+60 31 09		18.51 ± 0.04	16.62 ± 0.02	15.28 ± 0.01		8.20	0.22	M06
03 01 42.4	+60 31 28		18.04 ± 0.04	16.88 ± 0.03	15.99 ± 0.02		1.71	0.20	M06
03 01 30.6	+60 29 12		13.85 ± 0.05	12.79 ± 0.05	11.89 ± 0.04		0.25	0.27	M06
03 01 30.9	+60 29 19		14.30 ± 0.01	12.89 ± 0.01	11.86 ± <0.01		2.22	0.13	M06
03 00 57.2	+60 29 59		17.53 ± 0.03	16.19 ± 0.02	15.28 ± 0.01		4.04	0.12	M06
03 01 06.6	+60 30 11		18.15 ± 0.03	17.29 ± 0.03	16.68 ± 0.03		0.00	0.10	M06
03 01 06.0	+60 30 28		17.25 ± 0.01	16.26 ± 0.01	15.61 ± 0.01		1.29	0.06	M06
03 01 01.7	+60 30 41		16.81 ± 0.01	15.79 ± 0.01	15.06 ± 0.01		1.06	0.13	M06
03 01 00.9	+60 30 45		16.77 ± 0.01	15.64 ± 0.01	14.84 ± 0.01		2.02	0.13	M06
03 01 21.2	+60 30 11	03012120+6030105	15.88 ± <0.01	14.75 ± <0.01	13.97 ± <0.01		2.18	0.11	M06
03 01 20.2	+60 30 03		15.58 ± <0.01	14.31 ± <0.01	13.33 ± <0.01		2.51	0.23	M06
03 01 14.1	+60 29 38		17.37 ± 0.01	16.39 ± 0.01	15.59 ± 0.01		0.00	0.22	M06
03 01 16.5	+60 29 28		18.39 ± 0.03	17.39 ± 0.02	16.66 ± 0.02		0.78	0.14	M06
03 01 20.6	+60 29 28	03012059+6029280	17.02 ± 0.01	15.74 ± 0.01	14.82 ± 0.01		3.13	0.16	M06
03 01 19.1	+60 29 45		17.54 ± 0.01	16.27 ± 0.01	15.25 ± 0.01		2.19	0.27	M06
03 01 19.4	+60 29 39		17.73 ± 0.02	16.71 ± 0.01	15.93 ± 0.01		0.66	0.18	M06
03 01 19.1	+60 29 32		16.72 ± 0.01	15.69 ± 0.01	15.02 ± 0.01		1.68	0.06	M06
03 01 24.16	+60 29 21.3		18.52 ± 0.04	17.26 ± 0.04	16.47 ± 0.03		3.90	0.04	M06
03 01 24.90	+60 29 31.8		18.48 ± 0.04	17.02 ± 0.04	16.14 ± 0.03		5.94	0.02	M06
03 01 25.83	+60 30 15.1		19.26 ± 0.07	18.01 ± 0.06	17.20 ± 0.06		3.60	0.07	M06
03 01 26.13	+60 27 05.0		18.77 ± 0.05	17.96 ± 0.04	17.39 ± 0.06		0.00	0.09	M06
03 01 26.28	+60 28 34.5		19.44 ± 0.09	18.32 ± 0.06	17.63 ± 0.06		2.76	0.03	M06
03 01 28.85	+60 29 34.6		18.84 ± 0.05	17.55 ± 0.04	16.69 ± 0.03		3.75	0.10	M06
03 01 29.32	+60 29 23.9		17.27 ± 0.02	16.26 ± 0.01	15.60 ± 0.01		1.49	0.06	M06
03 01 29.38	+60 28 25.4		18.40 ± 0.03	17.38 ± 0.04	16.76 ± 0.03		1.94	0.02	M06
03 01 33.26	+60 29 33.7		18.44 ± 0.03	16.94 ± 0.03	16.05 ± 0.02		6.41	0.002	M06
03 01 33.92	+60 26 56.2		18.19 ± 0.03	17.33 ± 0.04	16.44 ± 0.03		0.00	0.38	M06
03 01 34.05	+60 29 28.6		18.20 ± 0.03	15.60 ± 0.01	14.00 ± <0.01	15.93	0.06	M06	
03 01 34.92	+60 29 27.5		16.91 ± 0.01	15.06 ± 0.01	13.92 ± <0.01	9.25	0.05	M06	
03 01 35.24	+60 28 55.7		17.65 ± 0.02	15.46 ± 0.01	14.15 ± <0.01	12.59	0.01	M06	
03 01 36.16	+60 28 41.0		16.58 ± 0.01	15.70 ± 0.01	15.17 ± 0.01	0.73	0.01	M06	
03 01 36.79	+60 31 27.8		18.29 ± 0.03	17.38 ± 0.04	16.78 ± 0.03	0.58	0.06	M06	
03 01 07.18	+60 30 04.0		18.84 ± 0.05	18.00 ± 0.06	17.37 ± 0.06	0.00	0.13	M06	
03 01 23.53	+60 31 50.7	03012352+6031507	16.154 ± 0.100	15.059 ± 0.088	14.313 ± 0.072	AAA 000	1.63	0.09	2MASS
03 01 05.21	+60 31 55.2	03010520+6031552	12.845 ± 0.023	11.905 ± 0.028	11.295 ± 0.022	AAA 000	0.75	0.04	2MASS
03 01 02.91	+60 31 22.4	03010291+6031223	15.942 ± 0.093	15.047 ± 0.104	14.421 ± 0.097	AAA 000	0.05	0.08	2MASS
03 01 27.22	+60 30 57.0	03012722+6030569	16.013 ± 0.084	15.047 ± 0.089	14.237 ± 0.057	AAA cc0	0.00	0.22	2MASS
03 01 02.92	+60 30 26.6	03010292+6030266	15.954 ± 0.086	15.062 ± 0.094	14.458 ± 0.103	AAA 000	0.18	0.06	2MASS
03 01 20.30	+60 29 49.3	03012029+6029493	11.991 ± 0.028	11.015 ± 0.030	10.154 ± 0.023	AAA 000	0.00	0.27	2MASS
03 01 18.60	+60 29 37.4	03011859+6029373	15.550 ± 0.081	14.785 ± 0.103	14.300 ± 0.084	AAA 000	0.00	0.01	2MASS
03 01 29.30	+60 31 13.6	03012930+6031136	14.346 ± 0.031	13.131 ± 0.037	12.320 ± 0.026	AAA 000	2.63	0.09	2MASS
03 01 17.70	+60 29 32.2	03011770+6029322	15.884 ± 0.084	15.112 ± 0.094	14.580 ± 0.091	AAA 000	0.00	0.05	2MASS
03 00 57.98	+60 31 21.8	03005798+6031217	16.033 ± 0.090	15.127 ± 0.092	14.533 ± 0.099	AAA 000	0.44	0.04	2MASS
03 01 21.86	+60 29 29.6	03012186+6029296	15.697 ± 0.065	14.734 ± 0.070	14.131 ± 0.071	AAA 000	1.10	0.02	2MASS
03 01 07.75	+60 29 21.9	03010774+6029218	14.249 ± 0.030	13.039 ± 0.033	12.212 ± 0.024	AAA 000	2.44	0.11	2MASS
03 00 57.92	+60 30 13.3	03005792+6030133	15.014 ± 0.046	13.931 ± 0.046	13.141 ± 0.039	AAA 000	1.12	0.14	2MASS
03 01 30.10	+60 29 55.5	03013009+6029554	14.529 ± 0.082	12.597 ± 0.062	11.379 ± 0.042	AAA ccc	8.49	0.11	2MASS
03 01 21.60	+60 28 56.7	03012159+6028566	11.788 ± 0.026	10.805 ± 0.030	9.869 ± 0.020	AAA 000	0.00	0.34	2MASS
03 01 00.92	+60 33 26.6	03010092+6033265	15.735 ± 0.076	14.863 ± 0.089	14.306 ± 0.098	AAA 000	0.31	0.02	2MASS
03 01 34.35	+60 30 08.7	03013435+6030087	14.782 ± 0.038	13.427 ± 0.035	12.560 ± 0.025	AAA 000	3.97	0.07	2MASS
03 01 31.88	+60 29 25.7	03013187+6029256	15.400 ± 0.049	12.921 ± 0.027	11.379 ± 0.018	AAA 000	12.85	0.13	2MASS
03 00 51.81	+60 32 10.7	03005180+6032106	15.903 ± 0.097	14.923 ± 0.101	14.253 ± 0.089	AAA ccc	0.77	0.08	2MASS
03 01 35.73	+60 28 49.0	03013572+6028490	14.867 ± 0.085	13.065 ± 0.060	12.017 ± 0.040	AAA cc0	8.20	0.01	2MASS
03 00 47.13	+60 28 53.5	03004713+6028535	15.105 ± 0.045	14.083 ± 0.057	13.369 ± 0.053	AAA ccc	0.96	0.10	2MASS
03 00 38.96	+60 32 29.6	03003896+6032295	15.893 ± 0.087	14.840 ± 0.081	14.185 ± 0.089	AAA 000	1.82	0.02	2MASS
03 01 44.84	+60 28 49.7	03014484+6028496	15.883 ± 0.105	13.863 ± 0.063	12.485 ± 0.045	AAA 000	8.33	0.22	2MASS
03 01 51.38	+60 27 22.5	03015137+6027224	15.672 ± 0.073	14.599 ± 0.071	13.885 ± 0.054	AAA 000	1.60	0.07	2MASS

Table 7 cont.

03 00 24.11	+60 32 36.3	03002411+6032363	16.195 ± 0.107	15.027 ± 0.104	14.213 ± 0.078	BAA	000	2.01	0.12	2MASS
03 02 00.11	+60 27 31.0	03020010+6027309	15.401 ± 0.056	14.244 ± 0.053	13.447 ± 0.042	AAA	000	2.01	0.11	2MASS
03 00 11.65	+60 31 20.2	03001164+6031202	16.000 ± 0.103	14.982 ± 0.082	14.258 ± 0.073	AAA	000	0.82	0.11	2MASS
03 01 01.33	+60 39 28.5	03010133+6039285	15.860 ± 0.092	14.942 ± 0.095	14.272 ± 0.093	AAA	000	0.00	0.11	2MASS
03 00 52.66	+60 39 31.8	03005265+6039317	15.043 ± 0.050	14.025 ± 0.050	13.291 ± 0.042	AAA	000	0.74	0.12	2MASS
03 01 05.81	+60 39 54.1	03010581+6039541	15.868 ± 0.088	15.040 ± 0.092	14.526 ± 0.092	AAA	000	0.09	0.002	2MASS
03 00 18.43	+60 36 41.9	03001843+6036419	15.687 ± 0.078	14.891 ± 0.080	14.272 ± 0.082	AAA	c00	0.00	0.13	2MASS
03 00 51.61	+60 39 48.9	03005161+6039489	15.270 ± 0.055	14.176 ± 0.044	13.478 ± 0.068	AAA	c00	2.00	0.04	2MASS
03 00 44.77	+60 40 09.2	03004476+6040092	14.683 ± 0.039	13.756 ± 0.039	13.008 ± 0.036	AAA	000	0.00	0.18	2MASS
02 59 54.51	+60 33 44.7	02595451+6033447	14.373 ± 0.047	13.387 ± 0.053	12.672 ± 0.040	AAA	000	0.49	0.12	2MASS
02 59 59.49	+60 26 42.1	02595949+6026421	15.212 ± 0.077	14.342 ± 0.081	13.777 ± 0.085	AAA	c0c	0.22	0.03	2MASS
02 59 44.48	+60 32 52.8	02594448+6032528	14.142 ± 0.035	13.216 ± 0.045	12.547 ± 0.033	AAA	000	0.09	0.10	2MASS
02 59 43.18	+60 33 32.0	02594317+6033319	15.851 ± 0.098	15.025 ± 0.095	14.390 ± 0.101	AAA	000	0.00	0.12	2MASS
02 59 42.82	+60 28 21.2	02594281+6028212	15.593 ± 0.075	14.647 ± 0.074	13.951 ± 0.080	AAA	c00	0.13	0.12	2MASS
02 59 40.85	+60 34 53.6	02594084+6034535	15.073 ± 0.050	13.995 ± 0.046	13.285 ± 0.039	AAA	000	1.70	0.06	2MASS
02 59 37.27	+60 34 18.4	02593726+6034183	15.666 ± 0.068	14.628 ± 0.087	13.886 ± 0.054	AAA	000	0.93	0.12	2MASS
02 59 30.10	+60 32 19.2	02593010+6032191	15.768 ± 0.086	14.852 ± 0.083	14.015 ± 0.072	AAA	000	0.00	0.28	2MASS
03 01 18.94	+60 44 25.7	03011894+6044257	9.597 ± 0.023	8.102 ± 0.040	7.204 ± 0.021	AAA	000	5.50	0.02	2MASS
02 59 26.32	+60 29 31.4	02592632+6029314	14.080 ± 0.031	13.042 ± 0.039	12.401 ± 0.023	AAA	000	1.74	0.02	2MASS
02 59 25.24	+60 32 51.9	02592523+6032518	14.001 ± 0.034	13.129 ± 0.035	12.514 ± 0.029	AAA	000	0.00	0.08	2MASS
02 59 17.55	+60 29 20.9	02591754+6029209	15.362 ± 0.050	14.589 ± 0.066	14.085 ± 0.069	AAA	ccc	0.00	0.02	2MASS
02 59 17.74	+60 34 03.6	02591773+6034035	15.526 ± 0.078	14.599 ± 0.082	14.020 ± 0.059	AAA	ccc	0.83	0.01	2MASS
02 59 16.00	+60 32 24.7	02591600+6032247	15.545 ± 0.067	14.475 ± 0.063	13.743 ± 0.056	AAA	000	1.42	0.09	2MASS
02 59 11.38	+60 31 40.2	02591138+6031401	14.289 ± 0.034	13.397 ± 0.037	12.804 ± 0.029	AAA	0c0	0.27	0.05	2MASS
02 59 11.73	+60 34 21.5	02591173+6034215	15.693 ± 0.079	14.805 ± 0.078	14.024 ± 0.057	AAA	000	0.00	0.24	2MASS
02 59 10.22	+60 33 40.8	02591022+6033408	15.320 ± 0.058	14.113 ± 0.049	13.276 ± 0.051	AAA	000	2.32	0.12	2MASS
02 59 06.34	+60 30 26.8	02590634+6030268	15.095 ± 0.059	14.253 ± 0.062	13.725 ± 0.055	AAA	ccc	0.16	0.01	2MASS
02 58 59.45	+60 31 18.6	02585944+6031185	14.081 ± 0.029	13.163 ± 0.035	12.596 ± 0.028	AAA	000	0.81	0.01	2MASS
02 59 02.05	+60 36 24.4	02590205+6036243	14.703 ± 0.037	13.726 ± 0.040	13.068 ± 0.033	AAA	000	0.83	0.07	2MASS
02 59 01.04	+60 38 15.0	02590104+6038149	15.557 ± 0.071	14.449 ± 0.077	13.735 ± 0.049	AAA	s00	2.05	0.05	2MASS
02 58 50.05	+60 30 51.6	02585004+6030516	13.505 ± 0.025	12.474 ± 0.033	11.639 ± 0.023	AAA	000	0.00	0.21	2MASS
02 58 44.68	+60 33 14.4	02584468+6033144	15.721 ± 0.075	14.893 ± 0.085	14.344 ± 0.074	AAA	000	0.00	0.04	2MASS
02 58 51.21	+60 39 54.4	02585120+6039544	15.218 ± 0.064	14.184 ± 0.062	13.487 ± 0.047	AAA	000	1.24	0.07	2MASS
02 58 53.70	+60 40 40.2	02585369+6040402	15.655 ± 0.080	14.601 ± 0.079	13.768 ± 0.058	AAA	000	0.41	0.20	2MASS
CMa R1										
07 04 01.24	-11 22 42.6	07040123-1122426	16.274 ± 0.094	14.936 ± 0.083	13.822 ± 0.054	AAA	000	1.77	0.33	2MASS
07 04 03.14	-11 23 27.6	07040314-1123275	13.033 ± 0.038	11.573 ± 0.037	10.694 ± 0.026	AAA	000	5.20	0.02	2MASS
07 04 05.19	-11 23 13.3	07040519-1123132	14.486 ± 0.071	13.265 ± 0.073	12.455 ± 0.040	AAA	000	2.72	0.09	2MASS
07 04 06.04	-11 23 15.6	07040603-1123156	15.113 ± 0.062	13.967 ± 0.044	13.247 ± 0.035	AAA	000	2.49	0.04	2MASS
07 04 01.21	-11 25 31.1	07040121-1125311	14.258 ± 0.032	12.963 ± 0.024	11.979 ± 0.021	AAA	000	2.26	0.22	2MASS
07 03 56.39	-11 25 41.4	07035638-1125413	15.717 ± 0.073	14.959 ± 0.070	14.422 ± 0.088	AAA	000	0.00	0.06	2MASS
07 04 09.96	-11 23 16.4	07040995-1123164	11.786 ± 0.024	10.709 ± 0.021	9.832 ± 0.021	AAA	000	0.35	0.23	2MASS
07 03 52.29	-11 21 00.9	07035228-1121009	15.705 ± 0.065	14.586 ± 0.068	13.777 ± 0.050	AAA	000	1.43	0.14	2MASS
07 04 09.26	-11 24 38.1	07040925-1124381	15.052 ± 0.039	14.250 ± 0.054	13.712 ± 0.053	AAA	000	0.00	0.04	2MASS
07 03 54.65	-11 20 11.0	07035465-1120110	15.933 ± 0.074	14.976 ± 0.076	14.368 ± 0.074	AAA	000	0.98	0.03	2MASS
07 04 05.77	-11 20 03.9	07040576-1120038	14.827 ± 0.048	13.459 ± 0.037	12.631 ± 0.030	AAA	000	4.44	0.02	2MASS
07 04 14.25	-11 23 16.9	07041424-1123169	13.896 ± 0.028	12.982 ± 0.022	12.341 ± 0.026	AAA	000	0.17	0.08	2MASS
07 04 14.28	-11 23 37.1	07041427-1123371	15.493 ± 0.064	14.579 ± 0.060	14.017 ± 0.059	AAA	000	0.80	0.003	2MASS
07 04 08.31	-11 20 05.3	07040831-1120052	13.600 ± 0.028	12.564 ± 0.026	11.919 ± 0.024	AAA	000	1.69	0.02	2MASS
07 04 15.00	-11 23 39.8	07041500-1123398	16.200 ± 0.086	15.049 ± 0.076	14.232 ± 0.075	AAA	c00	1.77	0.13	2MASS
07 04 12.16	-11 20 20.5	07041215-1120205	15.848 ± 0.072	14.463 ± 0.049	13.640 ± 0.040	AAA	000	4.70	0.01	2MASS
07 04 16.80	-11 24 32.4	07041680-1124324	14.123 ± 0.026	13.213 ± 0.028	12.595 ± 0.024	AAA	000	0.30	0.06	2MASS
07 04 05.98	-11 19 03.9	07040597-1119038	12.438 ± 0.029	11.045 ± 0.024	10.105 ± 0.019	AAA	000	3.86	0.12	2MASS
07 04 17.74	-11 24 03.8	07041774-1124037	15.108 ± 0.039	14.152 ± 0.038	13.567 ± 0.043	AAA	000	1.15	0.004	2MASS
07 04 09.22	-11 19 18.1	07040921-1119181	15.970 ± 0.068	14.526 ± 0.043	13.353 ± 0.035	AAA	000	2.64	0.33	2MASS
07 04 15.09	-11 26 22.4	07041508-1126224	14.151 ± 0.033	13.094 ± 0.032	12.441 ± 0.027	AAA	000	1.89	0.02	2MASS
07 04 19.99	-11 22 22.4	07041999-1122224	14.352 ± 0.029	13.340 ± 0.024	12.666 ± 0.029	AAA	000	1.15	0.06	2MASS
07 04 09.95	-11 18 25.2	07040994-1118251	12.995 ± 0.039	11.691 ± 0.034	10.503 ± 0.024	AAA	000	0.74	0.42	2MASS
07 04 12.33	-11 17 59.0	07041232-1117590	14.346 ± 0.029	13.309 ± 0.032	12.620 ± 0.030	AAA	000	1.35	0.06	2MASS
07 03 53.03	-11 29 35.3	07035303-1129352	12.356 ± 0.024	11.540 ± 0.022	10.947 ± 0.021	AAA	000	0.00	0.09	2MASS
07 04 13.46	-11 30 07.3	07041345-1130073	16.032 ± 0.079	15.048 ± 0.094	14.321 ± 0.084	AAA	000	0.37	0.13	2MASS
07 03 38.74	-11 29 16.4	07033874-1129163	15.395 ± 0.042	14.526 ± 0.070	13.976 ± 0.068	AAA	000	0.32	0.02	2MASS
07 04 20.87	-11 29 36.2	07042086-1129361	13.801 ± 0.024	12.883 ± 0.022	12.286 ± 0.024	AAA	000	0.57	0.04	2MASS
07 04 17.06	-11 30 37.0	07041706-1130370	13.705 ± 0.022	12.802 ± 0.026	12.247 ± 0.024	AAA	000	0.72	0.002	2MASS
07 04 34.08	-11 20 24.5	07043407-1120244	14.026 ± 0.035	13.038 ± 0.024	12.422 ± 0.027	AAA	000	1.31	0.02	2MASS
07 03 50.34	-11 32 51.4	07035034-1132514	15.812 ± 0.061	14.916 ± 0.086	14.297 ± 0.069	AAA	000	0.11	0.07	2MASS
07 03 50.43	-11 33 42.5	07035043-1133425	15.238 ± 0.056	14.395 ± 0.065	13.806 ± 0.057	AAA	000	0.00	0.07	2MASS

Table 7 cont.

07 03 45.54	-11 33 28.6	07034554-1133286	15.968 ± 0.079	14.597 ± 0.065	13.488 ± 0.038	AAA	ccc	2.23	0.30	2MASS
07 04 00.41	-11 33 59.6	07040041-1133596	12.099 ± 0.030	10.916 ± 0.028	10.190 ± 0.026	AAA	000	2.91	0.02	2MASS
07 04 01.60	-11 34 13.3	07040160-1134133	15.430 ± 0.052	12.449 ± 0.030	9.997 ± 0.026	AAA	000	11.94	0.77	2MASS
07 04 05.85	-11 34 10.0	07040584-1134099	16.174 ± 0.086	13.780 ± 0.043	12.195 ± 0.030	AAA	000	11.43	0.22	2MASS
07 03 58.50	-11 34 42.7	07035849-1134426	15.671 ± 0.070	14.552 ± 0.087	13.837 ± 0.055	AAA	000	2.18	0.05	2MASS
07 03 48.69	-11 34 30.3	07034869-1134303	15.658 ± 0.062	14.772 ± 0.066	14.182 ± 0.068	AAA	0cc	0.22	0.05	2MASS
07 03 56.67	-11 34 55.4	07035666-1134553	12.938 ± 0.024	11.872 ± 0.027	11.169 ± 0.023	AAA	000	1.60	0.06	2MASS
07 04 06.48	-11 34 47.1	07040648-1134470	15.009 ± 0.051	13.352 ± 0.065	12.365 ± 0.035	AAA	000	6.85	0.03	2MASS
07 04 36.12	-11 15 52.2	07043612-1115521	14.548 ± 0.037	13.237 ± 0.024	12.451 ± 0.027	AAA	000	4.06	0.01	2MASS
07 03 56.71	-11 35 09.6	07035670-1135095	14.336 ± 0.024	12.951 ± 0.027	12.114 ± 0.026	AAA	000	4.59	0.02	2MASS
07 03 55.43	-11 35 14.9	07035542-1135149	12.949 ± 0.026	11.970 ± 0.031	11.361 ± 0.027	AAA	000	1.25	0.02	2MASS
07 04 39.48	-11 32 35.6	07043947-1132356	15.023 ± 0.052	14.233 ± 0.045	13.688 ± 0.053	AAA	000	0.00	0.05	2MASS
07 04 33.95	-11 34 25.8	07043395-1134258	9.663 ± 0.024	8.295 ± 0.051	7.464 ± 0.023	AAA	000	4.42	0.03	2MASS
07 04 52.30	-11 14 30.6	07045230-1114306	12.720 ± 0.023	11.834 ± 0.024	11.285 ± 0.023	AAA	000	0.12	0.24	2MASS
07 04 01.80	-11 38 45.7	07040180-1138456	14.288 ± 0.030	13.263 ± 0.036	12.532 ± 0.025	AAA	000	0.55	0.01	2MASS
07 05 05.93	-11 17 45.8	07050593-1117458	14.220 ± 0.036	13.430 ± 0.042	12.896 ± 0.039	AAA	000	0.00	0.04	2MASS
07 05 16.42	-11 10 45.7	07051641-1110456	14.091 ± 0.076	12.691 ± 0.071	11.866 ± 0.054	AAA	ccc	4.87	0.002	2MASS
07 05 16.86	-11 10 43.8	07051685-1110437	12.153 ± 0.037	10.846 ± 0.036	9.806 ± 0.029	AAA	000	1.97	0.27	2MASS
07 05 18.78	-11 10 50.1	07051878-1110500	14.823 ± 0.038	13.940 ± 0.035	13.271 ± 0.032	AAA	000	0.00	0.13	2MASS
07 05 19.11	-11 10 26.9	07051911-1110269	15.305 ± 0.061	13.255 ± 0.039	12.022 ± 0.030	AAA	000	9.87	0.06	2MASS
07 02 27.04	-11 31 06.7	07022704-1131067	15.696 ± 0.065	14.842 ± 0.085	14.281 ± 0.080	AAA	000	0.00	0.09	2MASS
07 05 47.99	-11 17 43.7	07054798-1117436	15.877 ± 0.092	15.012 ± 0.075	14.466 ± 0.098	AAA	000	0.31	0.01	2MASS
07 05 45.29	-11 14 55.2	07054528-1114552	13.691 ± 0.030	12.857 ± 0.032	12.338 ± 0.026	AAA	000	0.13	0.004	2MASS
07 05 46.62	-11 15 45.2	07054662-1115452	15.890 ± 0.083	15.010 ± 0.071	14.459 ± 0.099	AAA	000	0.46	0.01	2MASS
07 06 00.79	-11 20 32.4	07060079-1120323	15.625 ± 0.091	14.740 ± 0.079	14.148 ± 0.084	AAA	000	0.19	0.05	2MASS
07 06 02.38	-11 26 54.2	07060238-1126541	12.302 ± 0.026	11.531 ± 0.028	10.974 ± 0.023	AAA	000	0.00	0.08	2MASS
07 06 12.23	-11 11 54.0	07061222-1111540	15.368 ± 0.050	14.538 ± 0.055	13.961 ± 0.055	AAA	000	0.00	0.06	2MASS